1 **Combining colour parameters and geochemical tracers to improve sediment source discrimination**

2 **in a mining catchment (New Caledonia, South Pacific Islands)**

3 Virginie Sellier[1] • Oldrich Navratil[2] • John Patrick Laceby[3] • Cédric Legout[4] • Anthony Foucher[1] •

4 Michel Allenbach[5] • Irène Lefèvre[1] • Olivier Evrard[1]

5 [1]Laboratoire des Sciences du Climat et de l'Environnement (LSCE), UMR 8212 (CEA/CNRS/UVSQ-IPSL),

6 Université Paris-Saclay, Gif-sur-Yvette (France)

7 [2] Laboratoire Environnement Ville Société (EVS), Université Lumière Lyon 2, UMR 5600 (CNRS), Lyon

8 (France)

9 [3] Alberta Environment and Parks, Calgary, Alberta (Canada)

10 [4]Institut des Géosciences de l'Environnement (IGE), UMR 5001, Grenoble (France)

11 [5]LIVE-EA 4243, Université de Nouvelle-Calédonie & LABEX Corail, Nouméa (Nouvelle-Calédonie,

12 France)

13 **Corresponding author:** selliervirg@free.fr ; Tel: (33)673910072

14   **Abstract**

15   Tracing the origin of sediment is needed to improve our knowledge of hydro-sedimentary

16   dynamics at the catchment scale. Several fingerprinting approaches have been developed to provide

17   this crucial information. In particular, spectroscopy provides a rapid, inexpensive and non-destructive

18   alternative technique to the conventional analysis of the geochemical properties. Here, we

19   investigated the performance of four multi-proxy approaches based on (1) colour parameters, (2)

20   geochemical properties, (3) colour parameters coupled with geochemical properties and (4) the

21   entire visible spectrum to discriminate sediment source contributions in a mining catchment of New

22   Caledonia. This French archipelago located in the south-west Pacific Ocean is the world's sixth-largest

23   producer of nickel. Open-cast nickel mining increases soil degradation and the downstream transfer

24   of sediments in river systems, leading to siltation of river systems. The sediment sources considered

25   in the current research were therefore sediment eroded from mining sub-catchments and non-

26   mining sub-catchments. To this end, sediment deposited during two cyclonic events (i.e. 2015 and

27   2017) was collected following a tributary design approach in one of the first areas exploited for nickel

28   mining on the archipelago, the Thio River catchment (397 km²). Source (n= 24) and river sediment

29   (n= 19) samples were analyzed by X-ray fluorescence and spectroscopy in the visible spectra (i.e. 365-

30   735 nm). The results demonstrated that the individual sediment tracing methods based on

31   spectroscopy measurements (i.e. (1) and (4)) were not able to discriminate sources. On the contrary,

32   the geochemical approach (2) did discriminate sources with 83.1 % of variance in sources explained.

33   However, it is the inclusion of colour properties in addition to geochemical parameters (3) which

34   provides the strongest discrimination between sources with 92.6 % of source variance explained. For

35   each of these approaches (2) and (3), the associated fingerprinting properties were used in an

36   optimized mixing model. The predictive performance of the models was validated through tests with

37   artificial mixture samples, i.e. where the proportions of the sources were known beforehand.

38   Although with a slightly lower discrimination potential, the 'geochemistry' model (2) provided similar

39   predictions of sediment contributions to those obtained with the coupled 'colour + geochemistry'

40   model (3). Indeed, the 'geochemistry' model (2) showed that mining tributary contributions

41   dominated the sediments inputs with a mean contribution of 68 ± 25 % for the 2015 flood event

42   whereas the 'colour + geochemistry' model (3) estimated that the mining tributaries contributed 65 ±

43   27 %. In a similar way, the contributions of mining tributaries were evaluated to 83 ± 8 % by the

44   'geochemistry' model (2) versus 88 ± 8 % by the 'colour + geochemistry' model (3) for the 2017 flood

45   event. Therefore, the use of these approaches based on geochemical properties only (2) or those

46   coupled to colour parameters (3) were shown to improve source discrimination and to reduce

47   uncertainties associated with sediment source apportionment. These techniques could be extended

48   to other mining catchments of New Caledonia but also to other similar nickel mining catchments

49   areas around the world.

51   **Keywords:** Nickel mining • Sediment source fingerprinting • Soil erosion • Modeling

1.Introduction

At the dawn of a fourth industrial revolution, demand for metalliferous minerals continues to increase and impact the world market (Prior et al., 2013;Highley et al., 2004). Currently, open-cast mining generates more than three-quarters of the world's metal ores. However, the extraction of these minerals is associated with deleterious impacts on the environment. In particular, these mines are responsible for the increase in soil erosion and the accelerated transfer of sediment in the river systems. Indeed, bare soil areas generated by mining activities including exploitation sites, prospection areas and access roads significantly increase runoff production (Yellishetty et al., 2013;Dumas et al., 2010;Abel et al., 2000). Moreover, the extraction of mineral ore is accompanied by a sharp production of mining wastes. Until the 1980s, no environmental regulation had been implemented to store this mining waste, and it was dumped directly onto the mountain slopes (Valette-Silver, 1993). Currently, this legacy mining waste provides an active source of sediment as it can progressively be remobilized (Coulthard and Macklin, 2003;James, 2013).

New Caledonia, an island located in the south-western Pacific Ocean and currently the world's sixth-largest producer of nickel, is in particular challenged with the problems of siltation of its river systems. Several studies outline how mining activities, which started in 1875, are generally responsible for these river morphological changes (Bird et al., 1984;Iltis, 1992;Garcin et al., 2017). In this case, excessive inputs of fine and coarse sediment triggered mainly during extreme rainfall events (e.g. cyclones and tropical depressions) have led to the disturbance of the sediment cascade in the river systems. A raising and widening of the riverbed has in particular been observed in the New Caledonian river systems by Garcin et al. (2017), leading to the increased occurrence of flooding events in these tropical regions. Owing to the occurrence of major cyclones in New Caledonia (i.e. on average one cyclone every 2.7 years (Garcin, 2010)), the local population regularly has to deal with the damage generated by these flood events: damage to human settlements, public infrastructure, agricultural land and human casualties. Moreover, suspended sediment is known to transport large

78   quantities of contaminants in river systems (Kumar and Maiti, 2015;Priadi et al., 2011;Varol, 2011).

79   Hedouin et al. (2007), and more recently Baudrimont et al. (2019), observed high concentrations of

80   trace metals, including Ni and Cr, in marine and freshwater organisms in New Caledonia. These

81   observations raise many questions about the health impact of mining activities on the populations

82   who eat a lot of fish. On a more global level, this anthropogenic activity also threatens the second

83   largest coral reef in the world, listed as a UNESCO World Heritage site (Davis and Fox, 2009). In

84   particular, the increased turbidity associated with sediment supply could disrupt coral metabolism

85   (i.e. photosynthetic processes) (Juillot, 2019). These coral reefs provide an exceptional biological

86   diversity and deliver several essential ecosystem services to the local population including fisheries,

87   coastal protection and tourism (Pascal, 2010). The implementation of effective and long-term

88   sediment control measures on mining sites (e.g. sediment retention basin, revegetation) is therefore

89   required to reduce sediment inputs into the lagoon. At this end, quantifying the sediment source

90   contributions from mining activities becomes particularly important as the mining industries are

91   subject to the "polluter pays" principle applied since 1975, i.e. the obligation to fund remediation

92   according to the extent of the damage generated by mining activity on the environment (Clarke and

93   David, 2010). Discriminating between sediment sources generated by mining activities and other

94   potential sediment sources is therefore a real social, environmental, political and financial challenge

95   in New Caledonia.

96   Indeed, other sediment sources that are not associated with mining activities as deforestation,

97   farming, pasture may contribute to sediment inputs in river systems. The use of fires to clear

98   landscapes also increases the area of bare soils (Dumas et al., 2010). Moreover, several invasive

99   species such as deers or wild pigs threaten soil stability through trampling and overgrazing (Shellberg

100   et al., 2010). Soils that are left uncovered with vegetation are more sensitive to erosion and they may

101   be exposed to landslides (Blake et al., 2009;Smith et al., 2011).

102   Sediment fingerprinting techniques have been developed since the 1970s to determine the

103 spatial origin of sediment sources and quantify their contributions (Klages and Hsieh, 1975;Walling et

104 al., 1979;Brown, 1985). These techniques are based on the analysis of multiple conservative

105 properties both in the sediments and their potential sources. The properties must necessarily be

106 conservative, i.e. the ranges of variation of these properties in the river material have to be

107 predictable based on those measured in the sediment sources. The ability of one or more of these

108 properties to discriminate between sources then allows to estimate the relative contribution of each

109 source through the use of a mixing model (Collins and Walling, 2002). Fallout radionuclides

110 (Wallbrink, 2004;Evrard et al., 2015;Wallbrink et al., 1998;Evrard et al., 2020), geochemical (Laceby

111 and Olley, 2015;Batista et al., 2018) and mineral properties (Gruszowski et al., 2003;Motha et al.,

112 2004) are the most frequently used tracers to quantify sediment source contributions. The use of

113 fallout radionuclides and geochemical properties as potential tracers was investigated to quantify the

114 sources of suspended sediment in the Thio River catchment (397 km²), one of the first catchments in

115 New Caledonia to be mined for nickel. Fallout radionuclides proved to be unsuitable (i.e. non-

116 discriminatory) while geochemical properties provided promising results, i.e. 83.1 % of variance

117 explained in sources (Sellier et al., 2019). The discrimination offered by geochemical properties was

118 particularly explained by the differences in geochemical composition outlined by Sevin (2014)

119 between the two dominant lithologies found in the archipelago: volcano-sedimentary formations

120 covering two thirds of the archipelago and peridotite massifs covering the remaining third where

121 mining activities are located. Mining erosion dominates 95 % of eroded areas identified on peridotite

122 massifs of the Thio River catchment according to the remote sensing study carried out by Garcin et

123 al. (2017). As a result, using geochemical properties is effective to indirectly quantify the sediment

124 contributions from mining activities and from areas devoid of mining activities. In this case, K

125 provides a straightforward tracer to discriminate the sediment sources (Sellier et al., 2019). Indeed,

126 volcano-sedimentary rock formations naturally contain high K elemental contents whereas peridotite

127 massifs are depleted in this element in New Caledonia (Sevin, 2014). Although these initial study

128 results were very promising, other less expensive, faster and possibly more efficient techniques than

129 the more conventional methods previously tested could be envisaged. For example, spectroscopy in

130 the mid-infrared (MIR) (Poulenard et al., 2009), the visible near-infrared (VNIR) and the shortwave-

131 infrared (SWIR) (Brosinsky et al., 2014) spectra have been used to quantify the sediment source

132 contributions. Spectroscopy is also non-destructive and requires low quantities of sample material.

133 Spectroscopy could therefore meet both the need for a simple, inexpensive, fast and portable

134 sediment tracing method in a context where flood events are frequent. This analysis technique could

135 also be more easily transferred to local populations so that they can carry out long-term

136 environmental monitoring of sedimentary contributions themselves.

137 Moreover, the geological specificity of the archipelago provides a strong contrast in terms of

138 soil colours observed either on the peridotite massifs or on the volcano-sedimentary formation rocks

139 and by extension, on the eroded sediments derived from these soils. On the one hand, the

140 weathering of peridotite massifs naturally enriched in Fe and transition metals such as Mn, Ni, Cr and

141 Co results in the formation of laterite profile composed of peridotites, saprolites, yellow laterites and

142 red laterites (from the bottom to the top). Hypermagnesian and ferrallitic ferritic soils that are rich in

143 goethite and hematite and that formed on the surface provide a particularly reddish-orange colour to

144 sediment derived from these exploited soils (i.e. mining sources, Figure 1) (Quantin et al.,

145 1997;Trescases, 1973). On the other hand, the weathering of volcano-sedimentary formation rocks

146 generates the formation of altered horizons rich in goethite and clay horizons rich in kaolinite (from

147 the bottom to the top) (Denis, 1988). The eroded sediment derived from fersialitic soils formed on

148 the surface is characterized by a yellow-grey colour (Figure 1). The differences made visually between

149 the two sources further encourage the analysis of sources by spectroscopy and especially

150 spectroscopy in the visible region of the spectrum (i.e. 365-735 nm). In particular, the colorimetric

151 parameters derived from the visible spectrum have been shown to be effective in discriminating

152 sediment sources. Their discrimination power has been tested both individually (Evrard et al.,

153 2019;Martínez-Carreras et al., 2010;Uber et al., 2019) and in combination with other tracers (e.g.

154   geochemical properties (Tiecher et al., 2015)) according to the conventional fingerprinting approach

155   (i.e. statistical analysis and use of a mixing model) (Collins et al., 1996). A more alternative approach

156   based on the entire visible spectrum with the partial least square regression (PLSR) models has also

157   been developed to trace origin of sediment sources in the literature (Legout et al., 2013;Tiecher et

158   al., 2015).

159
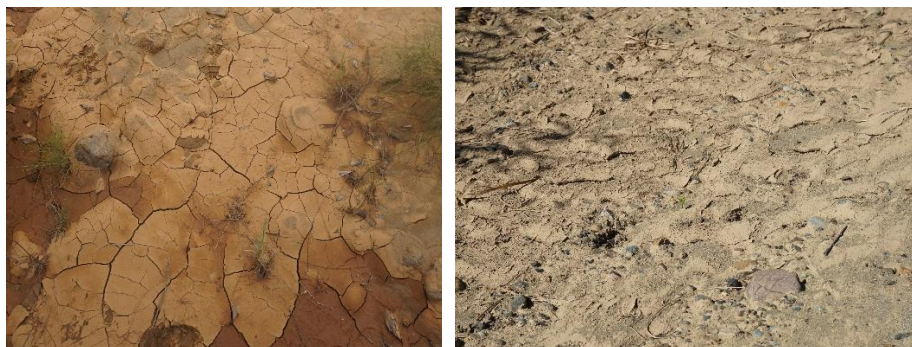
160   **Figure 1** Photographs of river material deposited on the channel banks of a mining tributary (left) and a
161   non-mining tributary (right) in the Thio River catchment

162   As part of this study, four sediment fingerprinting methods based on (1) colour parameters, (2)

163   geochemical properties, (3) colour parameters coupled with geochemical properties and (4) PLSR

164   models based on the whole visible spectrum were tested in the Thio River catchment. A tributary

165   design approach was implemented to trace the origin of sediments, i.e. sediment samples collected

166   on different tributaries were used as potential sources of the river sediment collected further

167   downstream on the Thio River (Laceby et al., 2017). Source (n=24) and river sediment (n=19) samples

168   were collected and analyzed by X-ray fluorescence and spectroscopy in the visible spectra (i.e. 365-

169   735 nm). For each of these sediment fingerprinting methods, the associated potential tracing

170   properties were used in an optimized mixing model. Tests with artificial mixture samples, i.e. where

171   the proportions of the sources were known beforehand were carried out to evaluate the predictive

172   performance of each model in order to select the best technique to be applied in the Thio River

173   catchment and possibly in other mining catchments of New Caledonia.

2.Materials and methods

2.1 Study area

Located in the southwestern Pacific Ocean, New Caledonia (18 500 km²) is made up of several islands, the largest of which is *La Grande Terre* (17 000 km²). The Thio River catchment (397 km²) is located on the east coast of this island (Figure 2-a). It has a mountainous relief, with an average altitude of 416 m above sea level (i.e. minimum: 0 m, maximum: 1392 m, Figure 2-a) and an average slope of 45 %. Two dominant lithologies are present in the catchment: volcano-sedimentary formations mainly located on the western part of the catchment and peridotite massifs concentrated in the eastern part of the catchment. Cherts (22 %), sandstone (9 %), a mix of basalt, dolerite and gabbro (6 %), polymetamorphic rocks (6 %) mainly constitute volcano-sedimentary formations whereas peridotite massifs are composed of laterites (18 %), peridotites (17 %), serpentines (10 %) and hazburgites (1 %) (Garcin et al., 2017) (Figure 1-b). The rock formation of these lithologies plays a key role in determining their degree of soil erodibility. In this case, Dumas (2010) described that volcano-sedimentary formations are less sensitive to soil erosion than peridotite massifs. Indeed, rocks from volcano-sedimentary formations such as basalts and cherts provide a certain resistance to erosion whereas laterites at the top of the profile are extremely sensitive to erosion processes, which explains why most forms of concentrated erosion (e.g. gullies, rills) and mass movements are mainly observed on peridotite massifs (Figure 3). However, the permanent vegetation covering 96 % of the Thio River catchment surface offers a relative protection against soil erosion across the catchment. Peridotite massifs naturally enriched in heavy metals have a low soil fertility, which explains why farming or pasture activities are not implemented on these soils (Quantin et al., 1997). Peridotite massifs have been exploited exclusively for their nickel resources since 1875. According to the mining registry, active and abandoned mining sites and exploration cover 21 % of the catchment area (Figure 2-c).

199   The Thio River catchment is subject to a tropical climate characterized by the alternation of a

200   hot wet season (November-April; mean temperature of 27 °C) and a cooler dry season (May-October;

201   mean temperature of 20 °C). The mean annual rainfall in the Thio River catchment is 1620 mm

202   despite strong seasonal fluctuations with the highest levels of precipitation recorded during the

203   cyclonic season between January and March (700 mm, 1981-2008; Alric (2009)). Although they only

204   occur on average once every 2.7 years, cyclones or tropical depressions may supply more than 20 %

205   of the annual rainfall in only one day according to local meteorological records (Météo France).

206

207   Twelve major tributaries flow into the main stem of the Thio River (28 km long) (Figure 2-b).

208   Ninety-two percent of the river channel length are characterized with slopes lower than 5 %.

209   According to Surell's classification (1841), the Thio River can be considered as torrential except in its

210   estuarine section. In addition, the longitudinal connectivity is exacerbated by the 8km² of bare soils

211   associated with past mining activities (~10 sites), ongoing mining operations (e.g. 2 sites: Thio

212   Plateau, Camps des Sapins) and the occurrence of 6 km² of mining roads. Bare soil areas increase soil

213   erosion processes on peridotites massifs, which once initiated, are difficult to contain (Figure3).

214   Heavy rainfall and the associated runoff exacerbate the widespread occurrence of rills, gullies,

215   landslides (Danloux and Laganier, 1991), thus contributing to connect the sediment sources to the

216   tributaries and consequently to the main river (Figure 3). For low intensity floods (i.e. <200 $m^3.s^{-1}$), a

217   strong remobilization of sediments in New Caledonian river systems has been observed (Allenbach et

218   al., 2020), thereby indicating that a lateral connectivity occurs in the Thio River catchment through

219   the occurrence of channel bank erosion.

220

221

a.

c.

b.
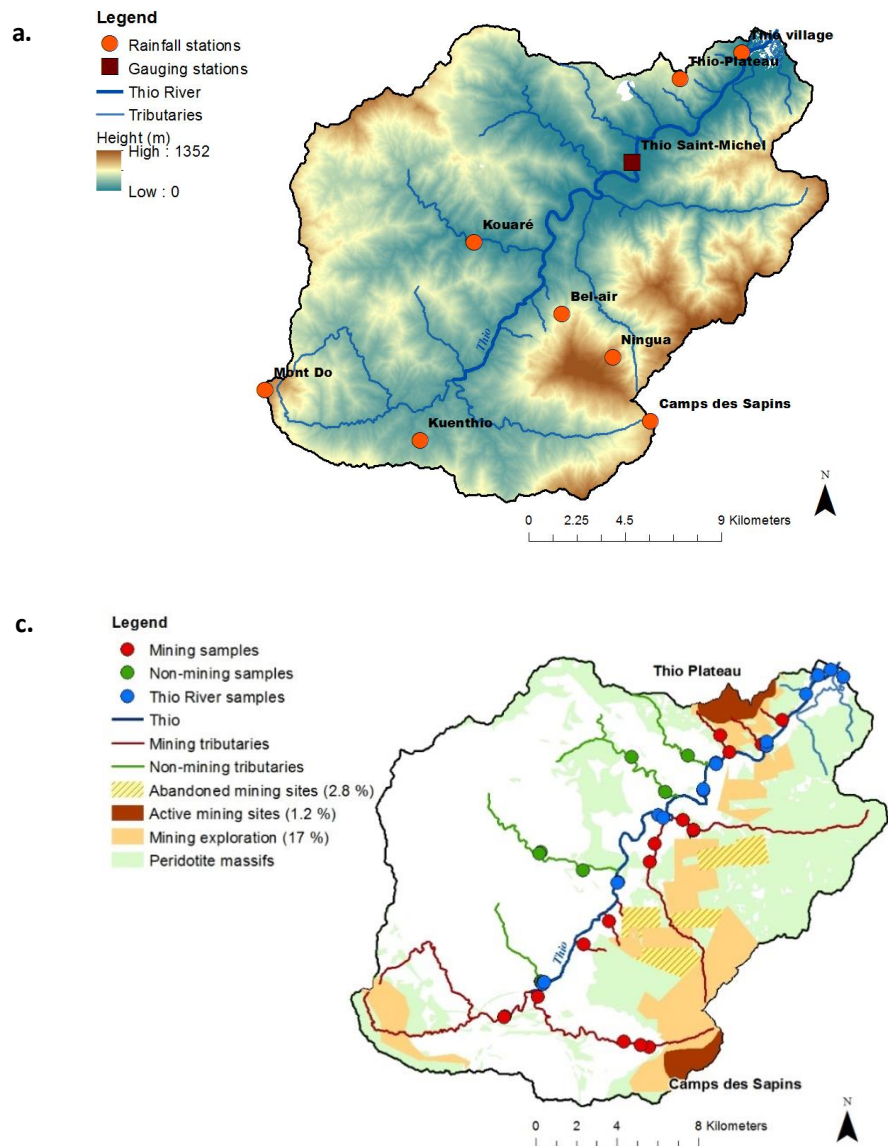
Figure 2 Location of the rainfall and river monitoring stations (a), main lithologies (b) and location of the sediment samples collected along with tributary source classifications (c) conducted in the Thio River catchment, New Caledonia

223

224

225 **Figure 3** Photographs of concentrated erosion and mass movement processes observed on peridotite
226 massifs of the Thio River catchment

227 **2.2 Hydro-sedimentary monitoring**

228   Three rainfall stations (Thio Plateau, Thio village, Camps des Sapins; Figure 2-b) are operated

229 by Météo France and five others are managed by the DAVAR (Direction des Affaires Vétérinaires

230 Alimentaires et Rurales; i.e. Kouaré, Bel-Air, Ningua, Kuenthio, Mont Do), with daily records available

231 since 1952 for some stations (e.g. Thio village). Daily discharge has been monitored at a river gauging

232 station located on the main stem of the Thio River (at Saint-Michel) since 1981 by the DAVAR (Figure

233 1-a).

234   **2.3 Sources and river sediment sampling**

235   In this study, two extreme events were investigated: Cyclone Murcia on February 25, 2015 and

236 Cyclone Cook on April 10, 2017. These cyclones respectively contributed to 7 % of annual rainfall in

237 2015 and 25 % in 2017. They generated floods with a return period of 10 years (i.e. 3500 $m^3.s^{-1}$). To

238 trace the origin of sediment, lag deposits were collected as an alternative of suspended sediment

239 sampling on channel bars of mining tributaries (n= 16), non-mining tributaries (n= 8) and the Thio

240 River (n= 19) according to the tributary design approach recommended by Laceby et al. (2017)

241 (Figure 2-c). Lag deposits were sampled after the two major floods generated by Cyclone Murcia (n=

242 31) and Cyclone Cook (n= 12). These two sample sets were respectively sampled between April 30

243 and May 5, 2015 and between May 16 and 17, 2017. At each sampling site, five to ten subsamples of

244 fine sediment were collected depending on the amount of observed sedimentary material. They

245 were sampled across a 10 m² surface with a plastic trowel at exposed subaerial sites free of

246 vegetation on channel bars. The subsamples were composited into one sample representative of the

247 fine sediment deposited on the channel bars. The samples were oven-dried at 40°C for ~48 hours.

248 Particle size selectivity may occur during the erosion, transport and deposition processes inducing an

249 overall finer particle size distribution in the river material compared to the sources. This selectivity

250 can lead to a non-conservation of the fingerprinting properties. For example, certain properties are

251 preferentially contained in a given particle size fraction which can create a relative enrichment or

252 conversely a relative depletion of these properties in the river material according to the particle size

253 fraction analyzed. In order to avoid this particle size effect, river sediment and source samples were

254 sieved to 63 μm, which is the most commonly used fraction in sediment tracing research (Owens and

255 Walling, 2002;Navratil et al., 2012).

256   **2.4 Preparation of artificial mixture samples**

257   Equal quantities of all mining tributary samples (0.4g for each sample, n= 16) were mixed

258 together to create a composite sample which would have an overall geochemical and colour

259 signature of the mining sources in the Thio River catchment (i.e. 'Mining source' pole). The same

260 process was carried out with non-mining tributary samples (0.4g for each sample, n= 8, 'Non-mining

261 source' pole). 'Mining source' and 'Non-mining source' pole samples were then mixed in known

262 proportions to create artificial mixture samples (n= 21, 0-100 % with a 5 % step, Table 1).

263

264 **Table 1** Proportions of mining and non-mining sources (%) in artificial mixture samples (M_i). *M6 was withdrawn*
265 *from this study because an error occurred at the time of its completion (not consider in the study).*

M_i	Proportions of 'mining source' pole (%)	Proportions of 'non-mining source' pole (%)
M1	0	100
M2	5	95
M3	10	90
M4	15	85
M5	20	80
M6	25	75
	(not consider in the study)	*(not consider in the study)*
M7	30	70
M8	35	65
M9	40	60
M10	45	55
M11	50	50
M12	55	45
M13	60	40
M14	65	35
M15	70	30
M16	75	25
M17	80	20
M18	85	15
M19	90	10
M20	95	5
M21	100	0

266

267 2.5 Source, river sediment and artificial mixture sample analyses

268   Spectroscopy measurements in the visible were carried out with a portable diffuse reflectance

269 spectrophotometer (Konica Minolta 2600d) at the Institut des Géosciences de l'Environnement (IGE,

270 Grenoble, France). To this end, between 0.1 g and 4 g of Thio River sediment (n= 19), source (n= 16)

271 and artificial mixture samples (n= 20) were stored in 60 mL polystyrene tubes. In order to perform

272 the analyses, the spectrophotometer was installed on a flat surface with the measuring window

273 facing upwards. The tubes were then placed on the 3-mm radius circle measuring cell. Because of the

274 rather small measuring area and to take into account the possible heterogeneity within the samples,

275 three measurements were carried out on river sediment and sources samples for each tube. For

276 artificial mixture samples, the experimenter who conducted the analyses performed four

277 measurements. Spectral reflectances were measured between 365 nm and 735 nm with a 10-nm

278 resolution. Several parameters were applied for each measurement: D65 illuminant, 10° angle

279 observer and specular component excluded. Raw data collected corresponds to the spectral

280 reflectance percentage for each of the 39-wavelength classes. From these raw data, 15 variables of

281 various colorimetry models were derived. Among these components, XYZ tri-stimulus values were

282 calculated based on the colour-matching functions defined by the International Commission on

283 Illumination (CIE 1931). The standardized tri-stimuli were then converted into CIELab and CIELu'v'

284 cartesian coordinate systems using the equations provided by CIE (1976) and then into CIELch,

285 CIEL*a*b* cartesian coordinate systems using the equations provided by CIE (1994) (Rossel et al.,

286 2006). First Derivative reflectance of the Visible Spectra (FDVS) of each sample was also derived from

287 the initial reflectance spectrum. According to Tiecher et al. (2015), the use of FDVS avoids differences

288 in baseline positions and allows to get rid of the small differences due to uncontrolled sources of

289 variation, as sample packaging. A zero and a white calibration were performed before each set of

290 measurements. In addition, and in order to evaluate a potential drift of the device's signal, control

291 measurements were carried with red, green, yellow panels and three contrasted sediment samples

292 before and after each set of measurements.

293   Measurements of 11 geochemical elements (i.e. Mg, Al, Si , K, Ca, Ti, Cr, Mn, Fe, Ni and Zn) on

294 the samples were conducted by pre-calibrated energy dispersive X-ray fluorescence spectrometry

295 (Epsilon 3, Malvern PANalytical) with certified reference samples including Internal Atomic Energy

296 Agency (IAEA) standards. Correlations between the determined and the standard elemental contents

297 were comprised between 0.90 and 0.99. The associated mean relative error was 9 % (SD 8 %).

298 Between 0.2 and 0.5 g of the samples were packed in small mass holder (SMH) cells with an air

299 double X-ray Mylar film and analyzed at the Laboratoire des Sciences du Climat et de

300 l'Environnement (LSCE, Gif-sur-Yvette, France). Samples were irradiated with a primary beam

301 generated by an Rh anode X-ray tube emitting electromagnetic waves between 100eV and 1MeV

302 with a maximum power, typical current and voltage fixed to 15 W, 3mA and 50 kV respetively. The

303 associated Si-drift detector had a Be window thickness of 8 μm and recorded the sample spectrum in

304 a 2D optical geometry configuration. X-ray intensities were converted into concentrations using the

305 Epsilon 3 software program through the application of the fundamental parameters method.

2.6 Statistical analysis and sediment tracing

2.6.1 Conventional mixing model

308 In general, the sediment source fingerprinting approach is composed of four main steps: (1)

309 range test, (2) the Mann-Whitney U test, (3) a stepwise discriminant function analysis and (4) a

310 mixing model (Collins et al., 1996;Laceby and Olley, 2015). For the range test, all variables exhibiting

311 values in the river sediment samples that were outside of the range found in the potential sources

312 (i.e. between the minimum and maximum values found in source samples) were excluded from the

313 analysis. It is important to restrict the tracing parameters to those that show a conservative behavior

314 to avoid incorrect source prediction and consequently inaccurate estimations of source contributions

315 (Sherriff et al., 2015). Thereafter, the Mann-Whitney U test ($\alpha = 0.05$, p-value <0.01) was performed

316 to evaluate whether conservative variables could discriminate mining tributary samples versus non-

317 mining tributary samples. A stepwise discriminant function analysis (DFA) was independently run on

318 three set of potential tracing properties: (1) colour parameters (i.e. 'colour'), (2) geochemical

319 properties (i.e. 'geochemistry') and (3) colour parameters and geochemical properties (i.e. 'colour +

320 geochemistry'). For the last set, the raw values of the variables were normalized in order to make

321 them comparable. Indeed, several colour parameters were within an order of magnitude of around

322 0.01 whereas for the geochemical parameters the difference was around 10^6 mg kg^{-1} which resulted

323 in a poorly conditioned matrix for the DFA.

324 The following calculation was therefore applied on the variable values to normalize them: x_i −

325 x_{min}/ x_{max} - x_{min} where xi was value found in source sample (i), x_{min} and x_{max} were respectively the

326 minimum and maximum values found in the source samples. The DFA was carried out to select the

327 optimal number of potential tracers to discriminate the sources for each modelling approach with

328 the optimal number of potential tracers which must provide the lowest Wilks' lambda value from

329 analysis of variance. Indeed, the closer the Wilks' lambda value is to 1, the lower the variability within

330 the sources compared to the total variability. The DFA was performed in the backward mode with a p

331 >0.01 used to select a tracer and p <0.01 used to remove a tracer. The *Statistica* software was used

332 to carry out the DFA because it has the advantage of automatically identifying and eliminating

333 collinear variables.

334   Finally, a classical solver-based mixing model was used to model the source contributions from

335 the mining and non-mining tributaries to target sediment through simultaneously minimizing the

336 mixing model difference (MMD) (Evrard et al., 2019):

$$MMD = \sum_{i=1}^{n} ((C_i - (A_i x + B_i (1 - x))/C_i) \quad Equation\ 1$$

337 where n is the number of parameters in the model chosen by the selection process (i.e. steps 1, 2, 3);

338 C_i is the Thio River sediment sample parameter (i); x and (1-x) were respectively the contributions of

339 source A and B (i.e. mining and non-mining tributaries); A_i is the mean of parameter (i) in source A

340 and B_i is the mean of parameter (i) in source B. The proportional contribution from each source (x)

341 was modelled by solving Equation 1 with the Solver Function in Microsoft Excel with x being between

342 0 and 1 and the sum of source contributions (i.e. x and 1-x) equaling 1. The GRG Non-Linear solving

343 method was used with automatic scaling in Solver, ignoring integer constraints, with a maximum run

344 time of 5000 and allowing for 2500 iterations. For each of the 2500 iterations, the values of the

345 variables were determined randomly with respect to their initially fixed ranges of values. A constraint

346 precision and convergence of $1.0\ 10^{-6}$ were selected for each of the model runs. To test the reliability

347 of the 'colour', 'geochemistry' and 'colour + geochemistry' models, these latter were tested on

348 artificial mixture samples.

    2.6.2   FDVS- PLSR model

350   FDVS-PLSR models were built following the methodology described in Poulenard et al. (2012).

351   The first step consisted in applying a principal component analysis (PCA) to evaluate the overall

352   variability between FDVS (i.e. 38-wavelength class) of source samples. Subsequently, a discriminant

353   analysis (DA) was conducted based on the PCA scores. The purpose of this analysis was to compare

354   the Mahalanobis distance between sources samples and to determine if FDVS of source samples

355   could discriminate the sources. Relationships between FDVS (x variate) and the corresponding weight

356   contribution of the sediment source data sets (y variate) were analyzed using PLSR. The PLSR models

357   were carried out based on the component set providing the lowest predictive error (PRESS, option on

358   XLStat software). Two independent PLSR models were built to estimate the two sediment source

359   contributions. As the artificial mixtures were measured four times by spectroscopy, 84 FDVS of

360   artificial mixture samples were generated including 50 values that were randomly selected to build

361   the models (training set (ST)) and 34 to validate the models (validation set (SV)). The SV:ST ratio used

362   was approximately 1:2, which is in agreement with recommendations provided in the literature

363   (Daszykowski et al., 2002). To evaluate the performance of PLSR models, several indicators such as

364   coefficient of linear regression (r^2), root mean square error of calibration (RMSEC) and root mean

365   square error of prediction (RMSEP) values were calculated. Unlike the conventional fingerprinting

366   approach, the estimated contributions of sources were not limited to be in the range of 0 % and 100

367   %. In a similar way, the sum of source contributions was not constrained to be equal to 100 %. As a

368   result, another way to control the reliability of predictions was to sum the prediction proportions of

369   both models (Legout et al., 2013). FDVS of river sediment samples were then introduced into these

370   PLSR models to estimate the contribution of sediment sources.

371 **3.Results**

372 **3.1 Source description**

373   The ranges of values of all colour parameters measured in the Thio River sediment samples

374 systematically plotted within the range of values observed in the two potential sources (i.e. mining

375 and non-mining tributaries; Figure 4 and Table 2). The range test results confirmed the conservative

376 character of these parameters. For geochemical properties, elemental concentrations measured in

377 the river sediment also plotted within the range of concentrations found in sources (Sellier et al.,

378 2019). In similar way, the range tests applied on geochemical properties showed that all these

379 properties were also conservative.

380
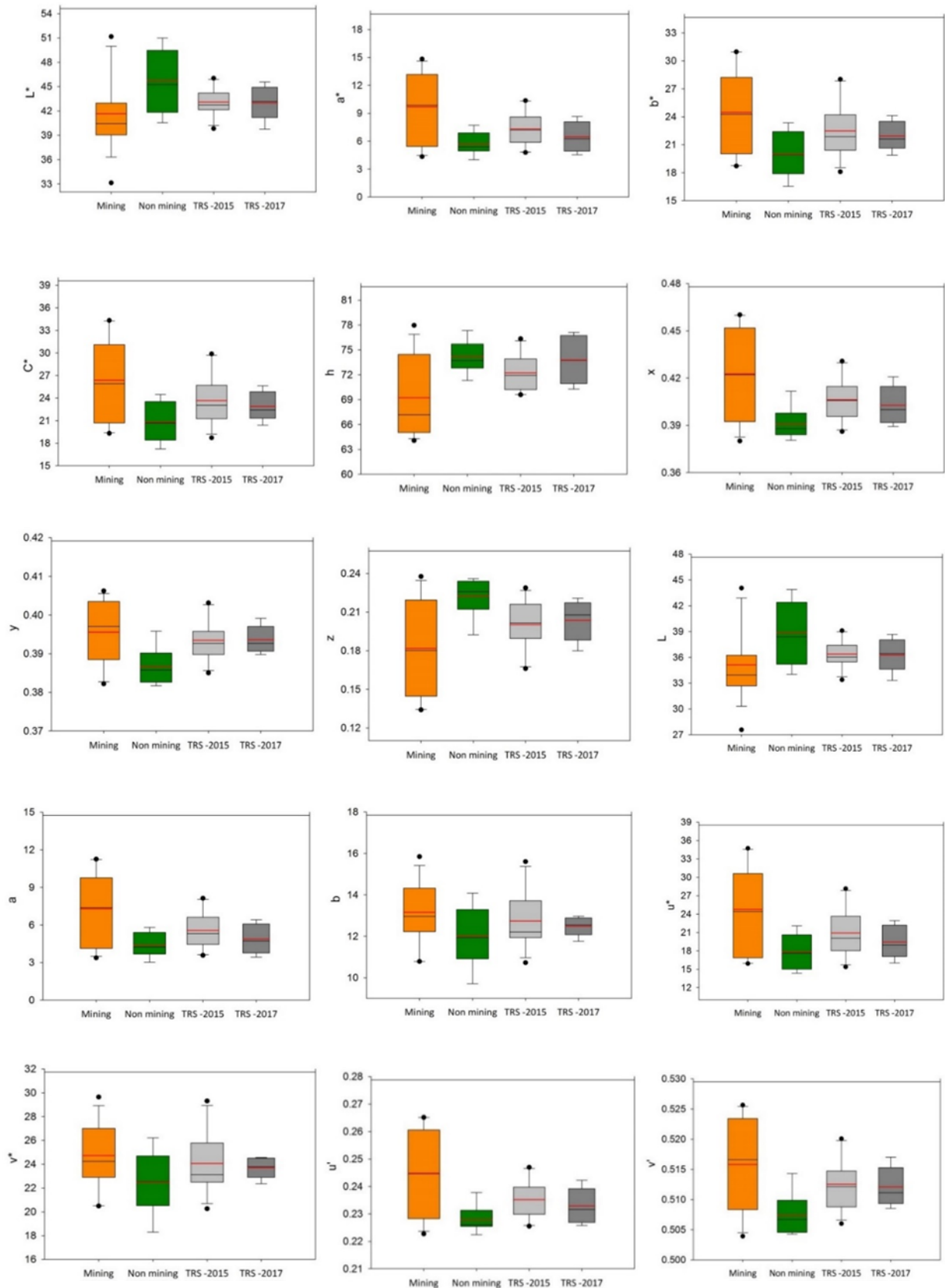
Figure 4 Box-plots of colour parameter values in the <63 µm fraction of sediment collected on the mining tributaries (Mining), non-mining tributaries (Non-mining) and the main Thio River (Thio River sediment (TRS)-flood events of 2015 and 2017). The box indicates the location of the first and third quartiles; the black line indicates the median value; the red line indicates the mean value

Table 2 Mean values of geochemical element contents and colour parameters in the <63 µm fraction of sediment sources and Thio River sediment (SD: standard deviation); results of Mann-Whitney U test and individual DA used to identify the potential tracers to differentiate sources supplying sediment to the Thio River

Fingerprinting property	Mann-Whitney U test *Mining tributaries versus non-mining tributaries*		DA- correctly classified samples (%)	Mean ± SD			
	U-value	p-value		Mining tributaries (n= 16)	Non-mining tributaries (n= 8)	Thio River sediment 2015 (n= 11)	Thio River sediment 2017 (n= 8)
Geochemical tracers							
Al *(g kg^{-1})*	8	0.000	87.5	21 ± 21	67 ± 8	43 ± 15	29 ± 6
Ca *(mg kg^{-1})*	21	0.007	62.5	3731 ± 470	9286 ± 5194	5281 ± 1201	3945 ± 666
Cr *(mg kg^{-1})*	124	< 0.0001	83.3	7480 ± 4606	706 ± 967	4359 ± 2185	5715 ± 1786
Fe *(g kg^{-1})*	121	0.000	91.6	144 ± 70	62 ± 24	43 ± 15	29 ± 6
K *(mg kg^{-1})*	2	< 0.0001	95.8	1657 ± 2160	14019 ± 3702	5944 ± 3294	3750 ± 974
Mg *(g kg^{-1})*	119	0.000	83.3	99 ± 59	16 ± 13	88 ± 33	117 ± 21
Mn *(mg kg^{-1})*	108	0.006	83.3	2531 ± 1317	1439 ± 606	2068 ± 667	1786 ± 516
Ni *(mg kg^{-1})*	125	< 0.0001	91.6	6576 ± 5075	358 ± 339	4218 ± 1938	4341 ± 1239
Si *(g kg^{-1})*	6	< 0.0001	91.6	178 ± 42	254 ± 28	221 ± 15	204 ± 7
Ti *(mg kg^{-1})*	13	0.001	87.5	1409 ± 2077	5446 ± 835	2771 ± 1197	1663 ± 457
Zn *(mg kg^{-1})*	68	0.834	-	146 ± 47	125 ± 4	134 ± 17	125 ± 8
Colour parameters							
L*	24	0.013	-	41.6 ± 4.6	45.7 ± 3.9	43.1 ± 1.7	43.0 ± 2.0
a*	104	0.013	-	9.7 ± 3.8	5.7 ± 1.2	7.3 ± 1.9	6.5 ± 1.7
b*	106	0.009	70.8	24.5 ± 4.5	20.0 ± 2.5	22.5 ± 3.0	21.9 ± 1.6
C*	108	0.006	66.6	26.4 ± 5.5	20.8 ± 2.7	23.7 ± 3.5	22.9 ± 2.0
h	26	0.019	-	69.2 ± 4.8	74.2 ± 1.9	72.2 ± 2.2	73.8 ± 2.9
x	107	0.007	75	0.42 ± 0.03	0.39 ± 0.01	0.41 ± 0.01	0.40 ± 0.01
y	111	0.003	79.2	0.396 ± 0.008	0.387 ± 0.005	0.393 ± 0.005	0.394 ± 0.004
z	19	0.005	75	0.18 ± 0.04	0.22 ± 0.01	0.20 ± 0.02	0.20 ± 0.02
L	27	0.013	-	35.1 ± 4.2	38.9 ± 3.7	36.4 ± 1.6	36.3 ± 1.9
a	103	0.016	-	7.3 ± 2.9	4.4 ± 1.0	5.6 ± 1.5	4.9 ± 1.2
b	91	0.106	-	13.1 ± 1.5	12.0 ± 1.5	12.7 ± 1.4	12.5 ± 0.4
u*	101	0.023	-	24.8 ± 6.9	17.8 ± 2.8	20.9 ± 4.0	19.4 ± 2.7
v*	93	0.081	-	24.7 ± 2.8	22.5 ± 2.7	24.1 ± 2.6	23.7 ± 0.8
u'	105	0.011	-	0.245 ± 0.016	0.228 ± 0.005	0.235 ± 0.007	0.233 ± 0.007
v'	111	0.003	79.2	0.516 ± 0.008	0.507 ± 0.004	0.513 ± 0.004	0.512 ± 0.003

3.2 Selection of parameters/properties for modelling

3.2.1 'Colour' model

According to the Mann-Whitney U test results, six colour parameters (*i.e.* b*, C*, x, y, z, v') provided significant discrimination between the two sediment sources (*i.e.* p-value < 0.01, Table 2). The backward DFA selected only v' as the optimal tracer of mining and non-mining source sediments (Figure 4, Table 3). Although this parameter correctly classified 79.2 % of sources, the high Wilk's lambda value obtained (i.e. 0.7209, Table 3) induced that only 27.9 % of variance was explained by v'. The low Mahalanobis distance value obtained (i.e. 1.6) confirmed that sediment sources were not well separated. Accordingly, and owing to the high error percentage of the source discrimination provided by this approach (i.e. 72.1 %), source contributions were not modeled with the 'colour' model.

3.2.2 'Geochemistry' model

When considering the two potential sediment sources, all geochemical properties (except Zn) were selected as potentially discriminant by the Mann-Whitney U test (i.e. p-value < 0.01, Table 2). Among the 10 potential tracers, K was selected by the backward DFA to model sediment source contributions from mining and non-mining tributaries with 95.3 % of sources correctly classified and 83.1 % of variance explained by K. This percentage of variance explained was deduced from the final Wilk's lambda value obtained (i.e. 0.1691). Moreover, the Mahalanobis distance value showed that the sediment sources were well separated from each other with a significant distance of 20.3 (Table 3) (Sellier et al., 2019).

3.2.3 'Colour + geochemistry' model

When combining colour parameters and geochemical properties, the DFA selected five optimal tracers (i.e. K, Ca, Ti, b*, C*) able to correctly classify 100 % of the sources. A significant improvement in the source discrimination was observed with the lowest Wilk's lambda value obtained (i.e. 0.0734)

and the highest percentage of variance explained (i.e. 92.6 %). Moreover, the Mahalanobis distance

value obtained (i.e. 52.1) was more than 2.5 times higher than that estimated with the

'geochemistry' model (Table 3), thus resulting in a better separation between sediment sources than

the previous approach (i.e. 'geochemistry')

Table 3 Results of DFA used to identify the optimum tracer combination to differentiate sources supplying
sediment to the Thio River

Fingerprint property selected	Wilks'Lambda	Variance explained by the variables (%)	Squared Mahalanobis distance	Correctly classified samples (%)
'Colour'				
v'	0.7209	27.9	1.6	79.2
'Geochemistry'				
K	0.1691	83.1	20.3	95.3
'Colour + Geochemistry'				
K, Ca, Ti, b*, C*	0.0734	92.6	52.1	100

3.3 Assessment of model performance on artificial mixture samples

Prior to applying mixing models to river sediments, preliminary tests were conducted to

control the validity of the models (i.e. 'geochemistry' and 'colour + geochemistry') and the associated

estimations of source contribution errors. When applying these models on the artificial mixture

samples, actual and predicted proportions were well correlated for both models (i.e. $r^2 = 0.99$ and $r^2 = 0.98$ respectively for 'geochemistry' and 'colour + geochemistry' models, $SD_{max} = 3$ %) (Figure 5).

However, the 'geochemistry' model described in Figure 5-a showed that the contributions of

mining tributaries were overestimated. With 100 % of actual mining contributions, 100 % of mining

contribution was predicted by the model. However, instead of 0 % of actual mining contributions, a

mining contribution of 15.5 % was predicted by the model. In other words, the more the estimated

mining source contributions tends towards 0 %, the greater the associated overestimation (i.e.

431 maximum 15.5 %) (Figure 5-a). The 'colour + geochemistry' model also provided a slight

432 overestimation of the contribution of mining tributaries (i.e. 7 % intercept of the regression line,

433 Figure 5-b). Given the slope of the regression line calculated is close to 1 (i.e. 0.98), this 7 %

434 overestimation remains constant over the entire range of potential contributions.
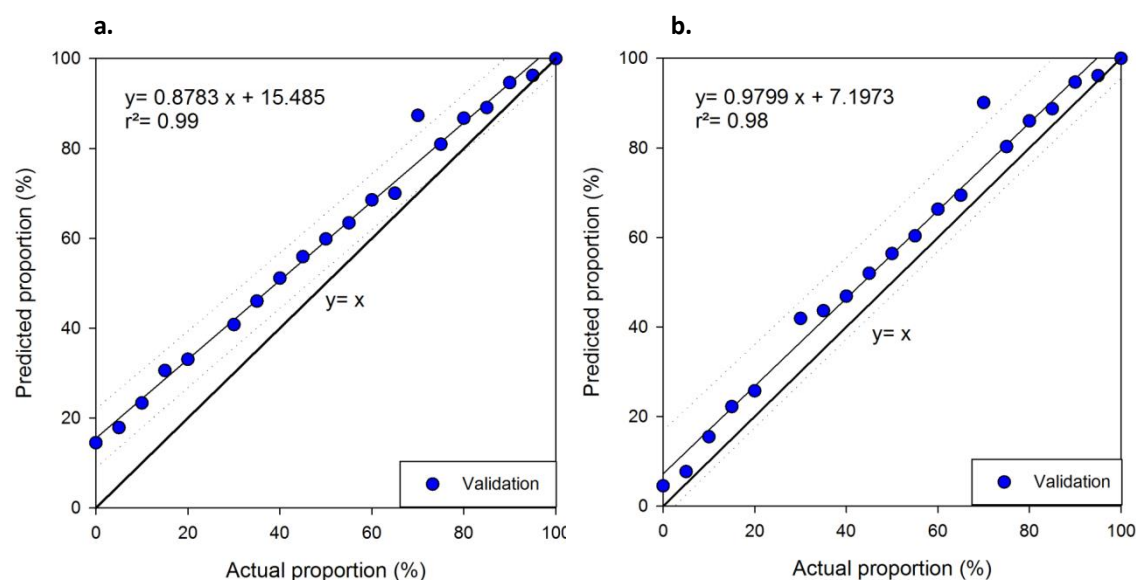
435 **Figure 5** Comparison between actual mining source proportions prepared in artificial mixtures and the mining
436 source proportions predicted by the 'geochemistry' (a) and 'colour + geochemistry' (b) models

437 **3.4 Building partial least-squares models based on FDVS**

438 Mining sources are characterized by a red-orange color while sediments originating from

439 non-mining sources are yellow-grey colour (Figure 1). The colour contrasts may be explained by the

440 distinct geochemical composition of these sources. Mean FDVS indicated the presence of goethite

441 (i.e. at 445 and 525 nm), hematite (i.e. at 555, 565 and 575 nm), and organic matter (i.e. between

442 600-700 nm) (Debret et al., 2011) in both mining and non-mining sources (Figure 6). In similar way,

443 the Thio River sediment samples (2015, 2017) showed similar characteristics since the variations of

444 the mean FDVS remained between those found in the sources (Figure 6). Nevertheless, some

445 differences can be observed between the sources. The spectral signature of goethite is slightly

446 stronger at 445 nm in non-mining tributaries compared to mining tributaries. No difference between

447 sources was observed at 525 nm, the second wavelengths characterizing the presence of goethite. In

contrast, the spectral signature of hematite (*i.e.* at 555, 565 and 575 nm) was stronger in mining tributaries than in non-mining tributaries.
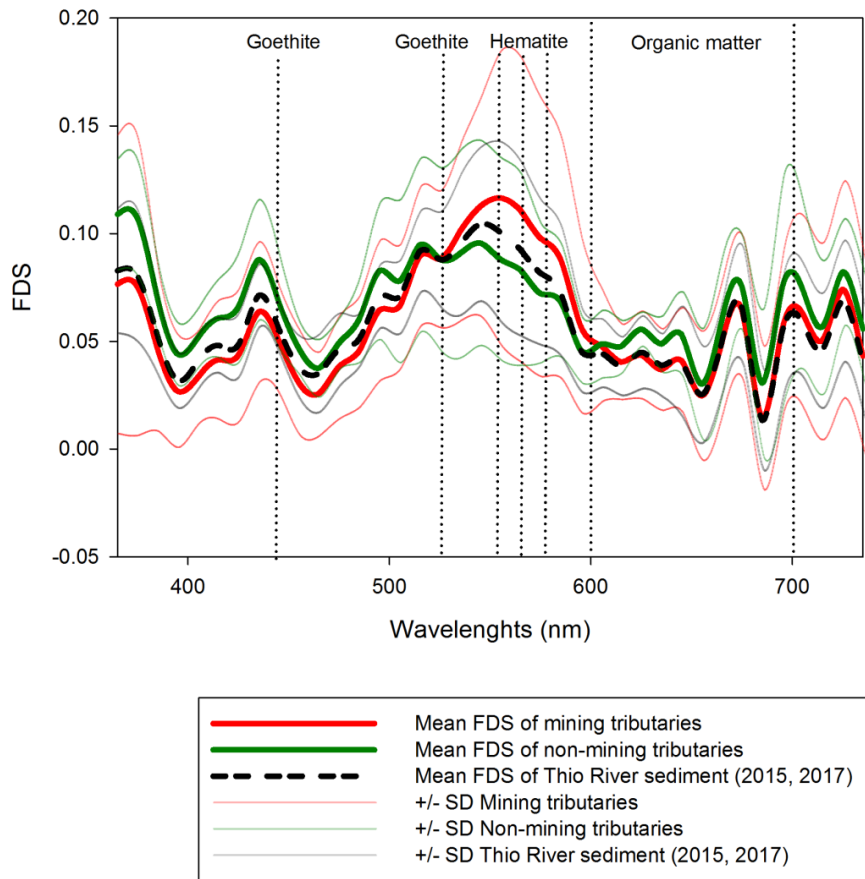
Figure 6 FDVS measured in the <63 µm fraction of sources and Thio River sediment samples

To test the potential discrimination offered by FDVS, a PCA was applied on the source data set. The first ten principal components from PCA explained 99 % of the total variation in the spectra. The DFA performed on these components resulted in a final Wilks' lambda value of 0.1585. In other words, 84.1 % of variance is explained by these ten components. Moreover, 100 % of the source samples were correctly classified. The performances of FDVS-PLSR models are presented in Figure 7. The mining and non-mining tributary FDVS-PLSR models provided an excellent correlation between actual and predicted proportions with r² and slopes close to 1 and intercepts of linear regression close to 0. The root mean square error of calibration (RMSEC) values estimated for both models were low, i.e. 3.4 % and 3.1 % respectively for mining (Figure 7-a) and non-mining tributary models (Figure

460 7-b). These models also provided a good predictability of source contributions with low root mean

461 square error of prediction (RMSEP) values (i.e. 8.0 % and 4.7 % respectively for mining and non-

462 mining tributary models). Another way to control the reliability of predictions was to sum the

463 predicted proportions of both models (Legout et al., 2013). Considering the whole data set used in

464 the construction of the partial least-squares regression models (i.e. calibration and validation) led to

465 a mean sum of the predicted source proportions of 102 % (SD 3 %, range: 98-114 %), thus

466 highlighting the effective prediction performance of FDVS-PLSR models.
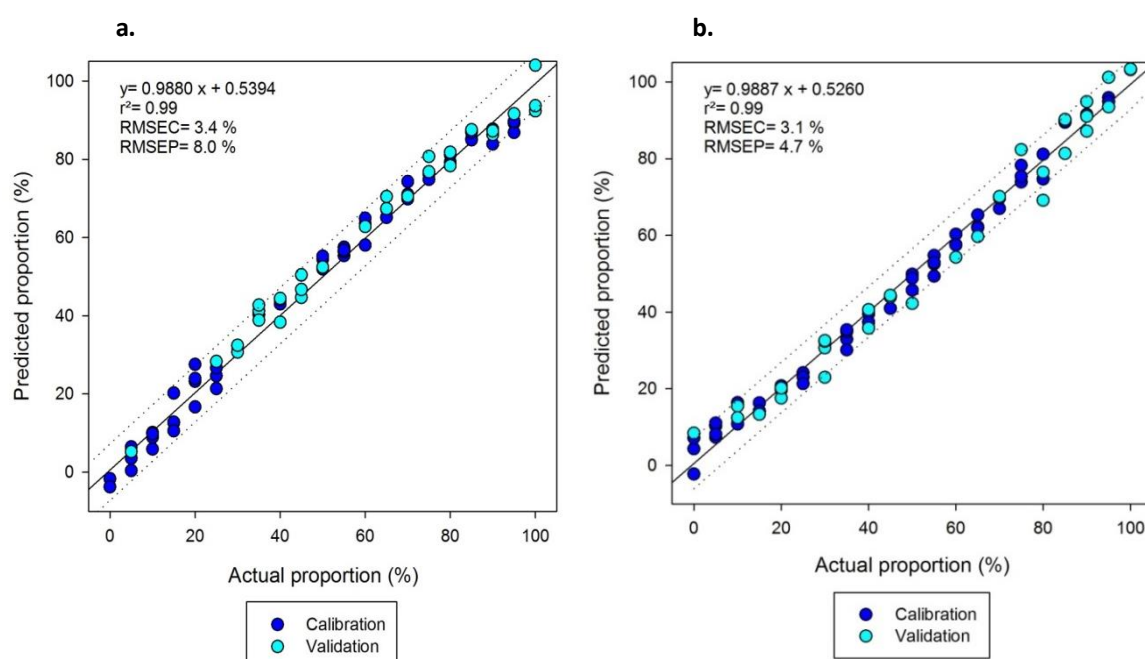
467   **Figure 7** Building of FDSV-PLSR models for mining sources (a) and non-mining sources (b)

468   **3.5 Source apportionment modelling**

469   3.5.1   'Geochemistry' model

470   The 'geochemistry' model estimated that the mining tributaries contributed an average of 65

471 ± 27 % of the Thio River sediment during the 2015 flood event; they therefore dominated sediment

472 inputs overall during this event. Nevertheless, non-mining tributaries mainly contributed to the

473 sediment inputs at three sampling points along the Thio River (Figure 8-a, Table 4, sampling points [3,

474 5, 7]). These contributions did not, however, compensate for those provided by mining tributaries in

475 the estuary (63-89 %). Indeed, the dominant mining contributions found in upstream river reaches

476 (96 %, Figure 8-a, Table 4, sampling point [1]) gradually decreased along the Thio River, fluctuating

477 between 17-77 % before increasing again at the confluence between the Thio River and the mining

478 tributaries draining the Thio Plateau mining area (i.e. 85 %, Figure 8-a, Table 4, sampling point [8])

479 and reaching 60-64 %.

480

481   The 'geochemistry' model also demonstrated that mining tributaries dominated sediment

482 inputs with a mean contribution of 83 ± 8 % during the 2017 flood event (Table 5). The lowest mining

483 tributary contributions estimated (i.e. 69 %) was found after the confluence with the Kouaré non-

484 mining tributary (Figure 8-b, Table 5, sampling point [4]). Nevertheless, further downstream, the

485 proportions of the mining sources increased again to reach 77-83 % in the estuary (Figure 6-b, Table

486 5, sampling points [7, 8]).

487
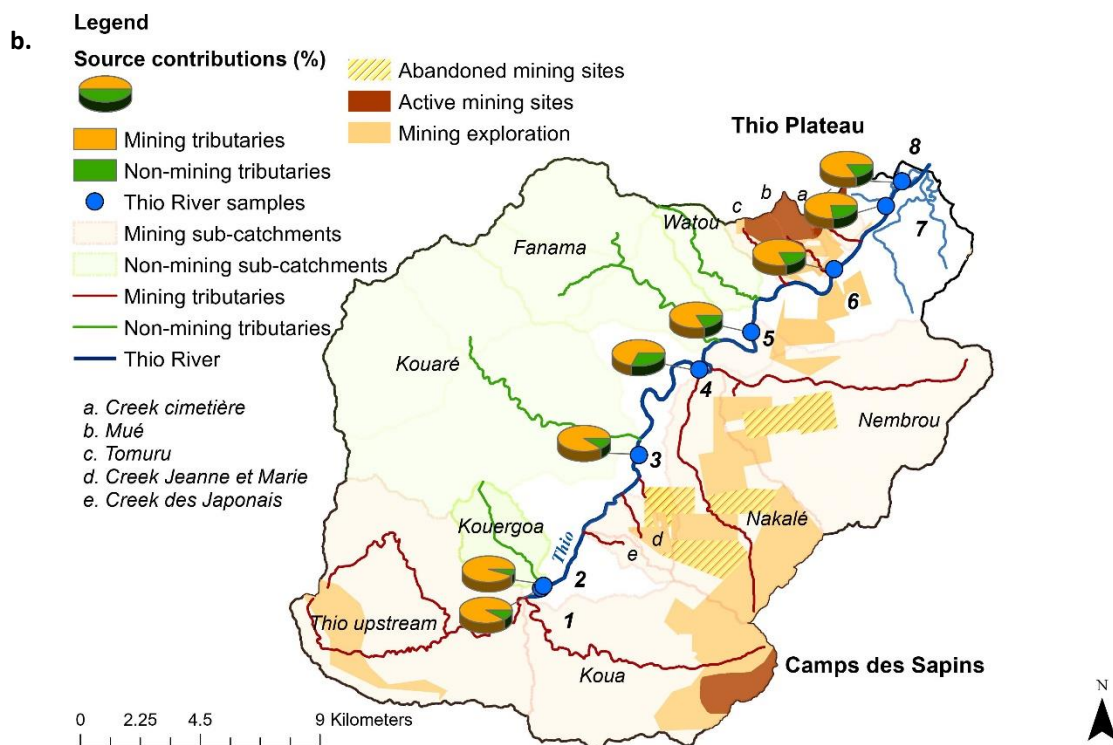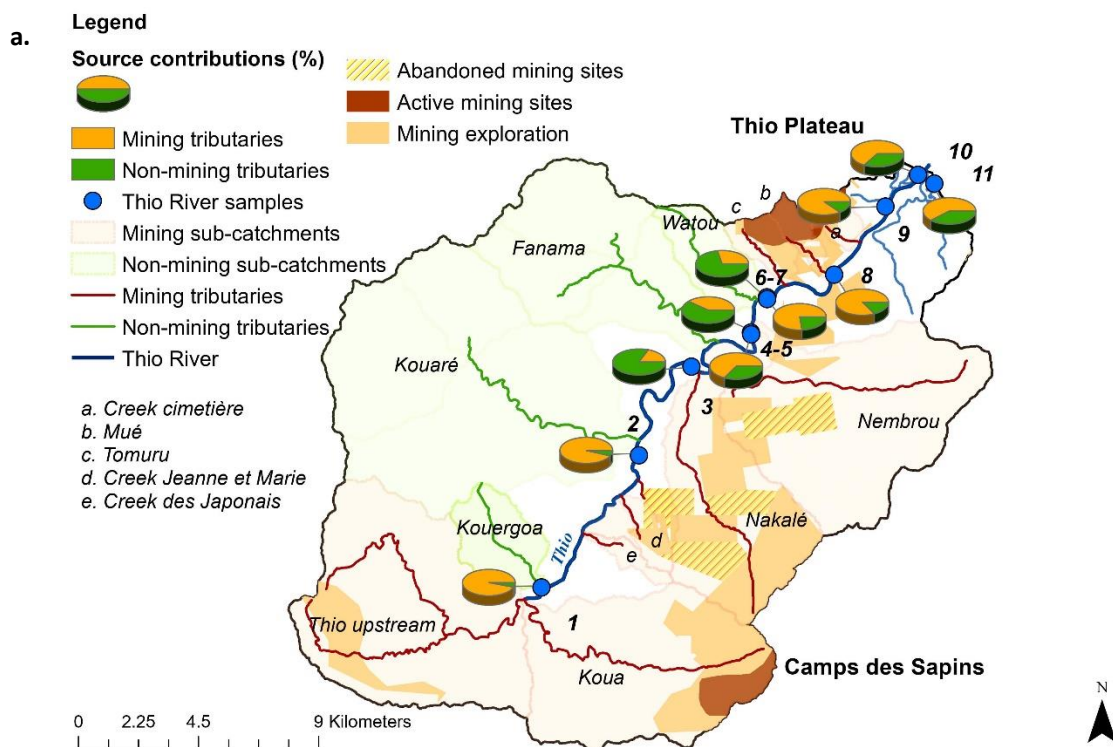
Figure 8 Relative contributions of mining and non-mining tributaries to the sediment collected in the Thio River during the 2015 (a) and 2017 (b) flood events using the 'geochemistry' model

494   3.5.2   'Colour + geochemistry' model

495   Similar results were obtained with the 'colour + geochemisty' model. The contributions of

496   mining tributaries were estimated to an average of 68 ± 25 % for the 2015 flood event. Mining

497   tributary contributions provided almost all the sediment transiting the uppermost reach of the Thio

498   River (i.e. 99 %, Figure 9-a, Table 4, sampling point [1]). However, after the confluence with the

499   Kouaré tributary, non-mining tributaries dominated with a contribution of 83 % (Figure 9-a, Table 4,

500   sampling point [3]). Further downstream, the contribution of mining tributaries increased again with

501   supplies varying between 34- 89 % to reach 58- 70 % in the estuary (Figure 9-a, Table 4). The largest

502   difference between 'geochemistry' and 'colour + geochemistry' model outputs was 18 % for the 2015

503   flood event.

504   The 'colour + geochemistry' model also demonstrated that 88 ± 8 % of the sediment supply

505   originated from mining tributaries during the 2017 flood event. Along the Thio River, mining tributary

506   contributions varied between 100 % in the uppermost reach, 74 % after the Kouaré river confluence

507   and 83-85 % in the estuary (Figure 9-b, Table 5). The largest difference between 'geochemistry' and

508   'colour + geochemistry' model outputs was 10 % for the 2017 flood event (Table 5).

509
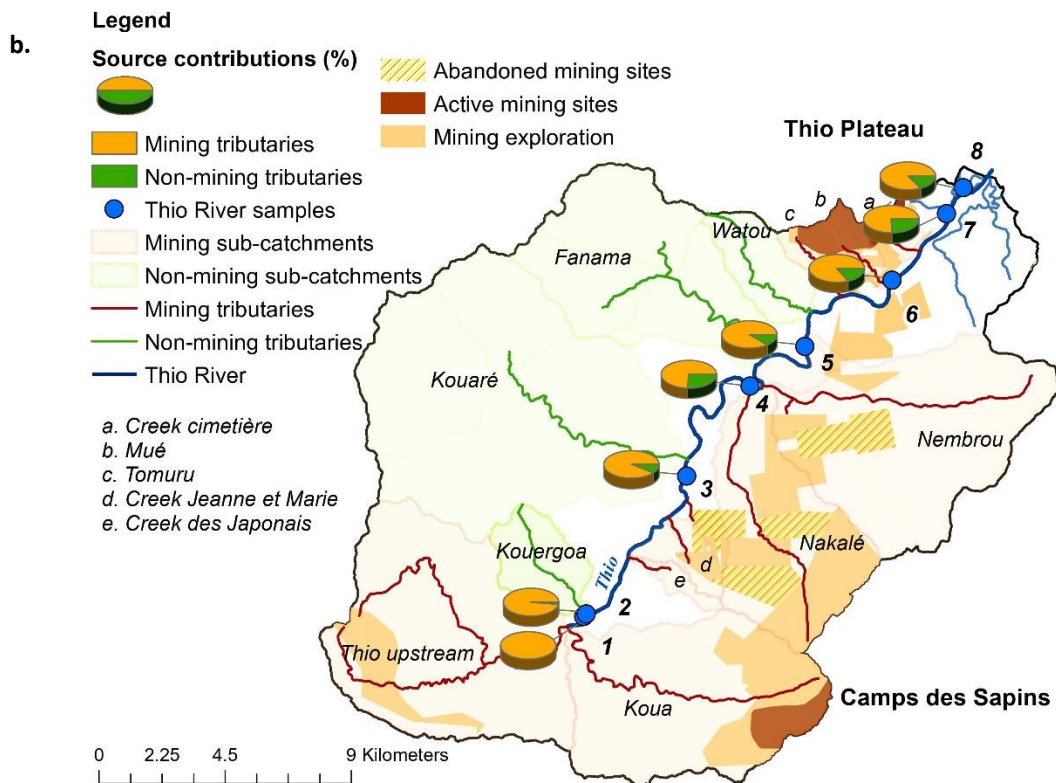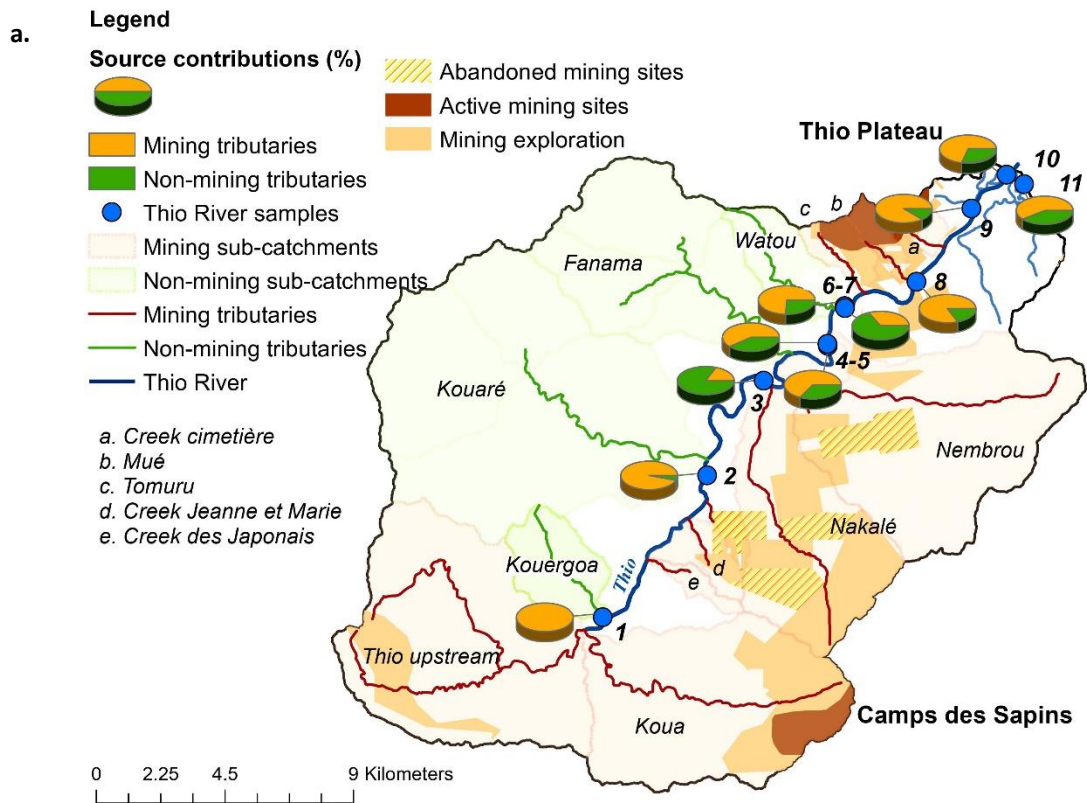
Figure 9 Relative contributions of mining and non-mining tributaries to the sediment collected in the Thio River during the 2015 (a) and 2017 (b) flood events using the 'colour + geochemistry' model

3.5.3 FDVS-PLSR model

Unlike the conventional fingerprinting approach, the estimated contributions of sources were not limited to vary in the range between 0 % and 100 %. In a similar way, the sum of source contributions was not constrained to be equal to 100 %. As a result, another method to control the reliability of predictions was to sum the predicted proportions of both models and to verify that this sum was close to 100 % with an acceptable error of ± 20 %. If this point is not verified, it is likely that a potential source has not been sampled and considered in the study or that the behaviour of the fingerprinting properties is not conservative (Legout et al., 2013). When applying the FDVS-PLSR models (i.e. mining and non-mining tributary contributions) to the river sediment samples (2015, 2017), the mean sums of the source contributions were 92 ± 8 % and 80 ± 13 %, respectively, for the 2015 and 2017 flood events (Tables 4 and 5) which are satisfactory results. However, for the 2017 flood events, three river sediment samples collected on sampling points n°1, 2 and 3 showed sums of source contributions below 70 %, indicating a lack of reliability of the model. The results obtained on these three points must therefore be interpreted with great caution. Moreover, and owing that predicted sums were slightly different from the expected 100 %, a bar plot display of the source contributions has been chosen to facilitate the interpretation of the results (Figure 10).

According to the FDVS-PLSR model results, 34 ± 22 % of sediment supply originated from mining tributaries while non-mining tributary contribution provided 58 ± 18 % of the sediment input for the 2015 flood event (Figure 10-a, Table 4). In the upper part of the Thio River catchment, non-mining tributaries largely dominated with a contribution of 80 % versus 6 % for mining tributaries. Along the Thio River, mining tributary contributions gradually increased to reach 70 % after the Mué tributary confluence (i.e. one of tributaries draining the Thio Plateau Mine, Figure 8-a, Table 4, sampling point [9]). The non-mining tributary contributions fluctuated along the Thio River between 41-85 % (Figure 8-a, Table 4, sampling points [2-8]) and reached a minimum to 28 % (Figure 10-a, Table 4, sampling point [9]) after the Mué tributary confluence. In the estuary, sediment supply was

540   originated from 51-70 % of mining tributaries and 28-52 % of non-mining tributaries (Figure 10-a,

541   Table 4, sampling points [9, 10, 11]).

542   The FDVS-PLSR models also indicated that mining and non-mining tributaries respectively

543   contributed a mean of 29 ± 20 % and 51 ± 11 % of sediment (Figure 10-b, Table 5) during the 2017

544   flood event. In a similar way, mining contributions gradually increased along the Thio River from 11 %

545   in upper parts to reach 52-58 % in the estuary. On the contrary, non-mining contributions gradually

546   decreased from 56 % in uppermost parts to reach 35-36 % in the estuary (Figure 10-b, Table 5).

547   In summary, the FDVS-PLSR models provided opposite results to those of the conventional

548   sediment fingerprinting approach (i.e. 'geochemistry' and 'colour + geochemistry' models). According

549   to the FDVS-PLSR models, non-mining tributaries contributed the majority of the sediment supply for

550   the 2015 (58 ± 18 %) and 2017 (51 ± 11 %) flood events. On the contrary, the 'geochemistry' and

551   'colour + geochemistry' models demonstrated that mining tributary contributions dominated

552   sediment supply for the 2015 (i.e. respectively 65 ± 27 % and 68 ± 28 %) and 2017 flood events (i.e.

553   respectively 83 ± 8% and 88 ± 8%).

554
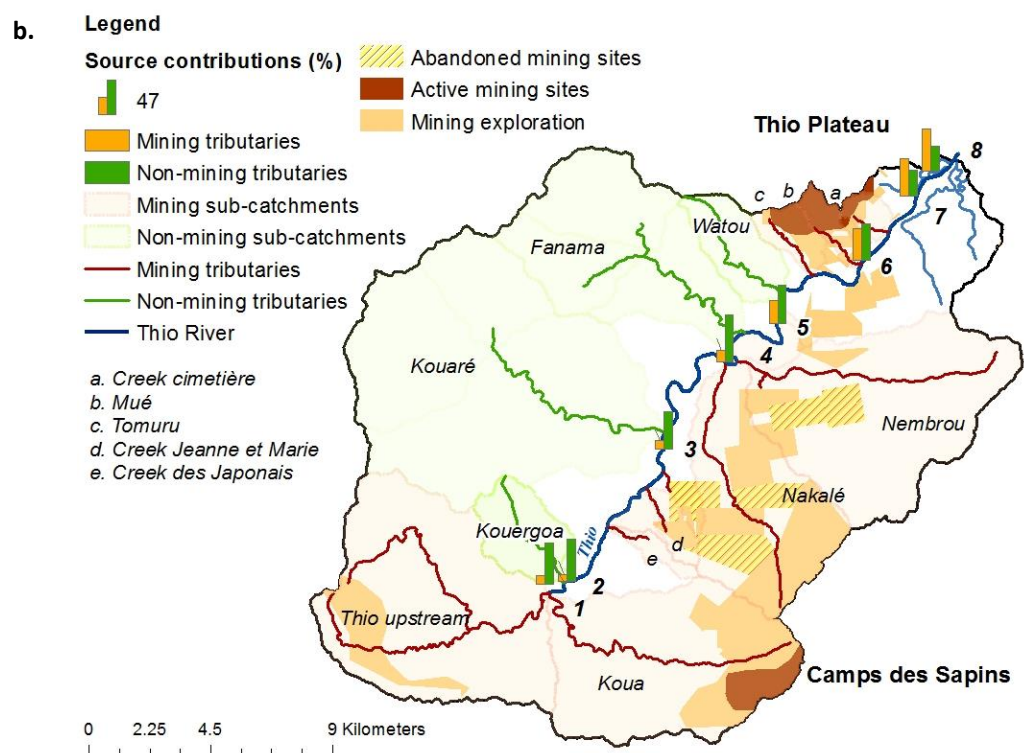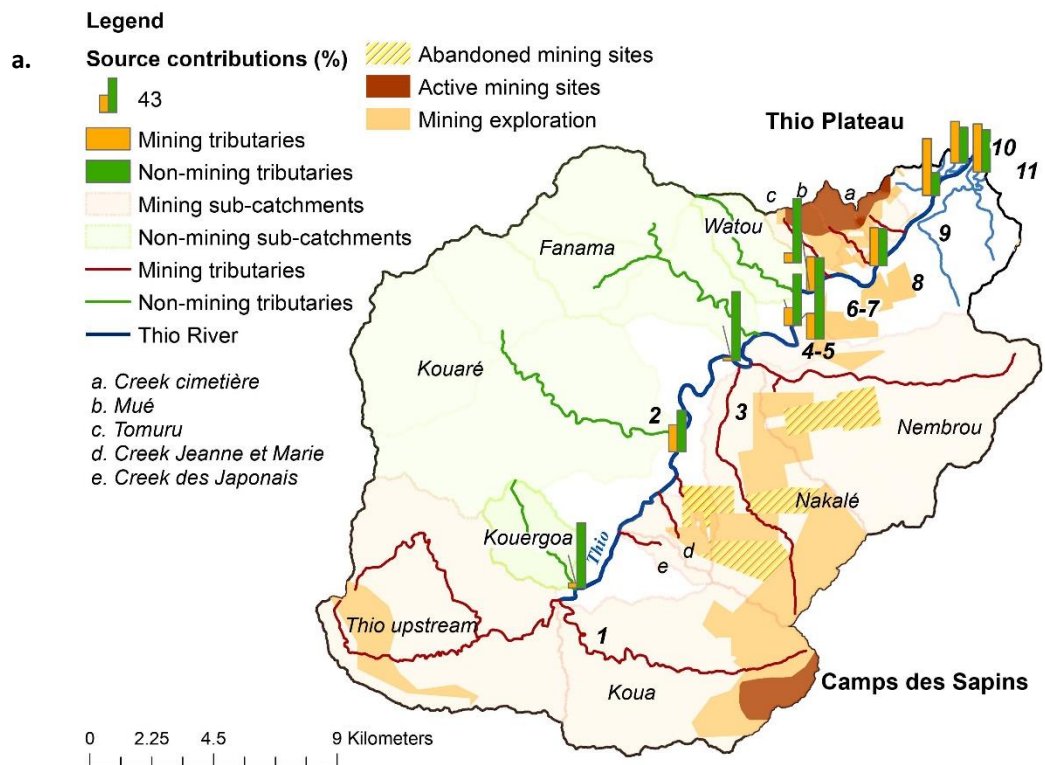
Figure 10 Relative contributions of mining and non-mining tributaries to the sediment collected in the Thio River during the 2015 (a) and 2017 (b) flood events using the FDVS-PLSR models

Table 4 Source contributions calculated by FDVS-PLSR, 'geochemistry', 'colour + geochemistry' approaches for sediment deposited during the flood of February 25,2015

561 (Mean, SD: standard deviation, minimum, maximum)

Sampling point	Mining tributary contributions (%)			Non-mining tributary contributions (%)			Sum of source contributions (%)		
	FDVS- PLSR	Geochemistry	Colour + Geochemistry	FDS- PLSR	Geochemistry	Colour + geochemistry	FDS- PLSR	Geochemistry	Colour + geochemistry
1	6	96	99	80	4	1	86	100	100
2	33	95	96	51	5	4	84	100	100
3	4	17	17	85	83	83	90	100	100
4	32	65	65	64	35	35	96	100	100
5	22	41	59	63	59	41	85	100	100
6	42	77	74	41	23	26	83	100	100
7	12	29	34	79	71	66	91	100	100
8	47	85	83	46	15	17	93	100	100
9	70	88	89	28	12	11	98	100	100
10	51	64	70	44	36	30	94	100	100
11	59	60	58	52	40	42	111	100	100
Mean (%)	34	65	68	58	35	32	92	100	100
SD (%)	22	27	25	18	27	25	8	-	-
Minimum (%)	4	17	17	28	4	1	84	-	-
Maximum (%)	70	96	99	85	83	83	111	-	-

565   **Table 5** Source contributions calculated by FDVS-PLSR, 'geochemistry', 'colour + geochemistry' approaches for sediment deposited during the flood of April 10,2017 (Mean,

566   SD: standard deviation, minimum, maximum)

Sampling point	Mining tributary contributions (%)			Non-mining tributary contributions (%)			Sum of source contributions (%)		
	FDVS-PLSR	Geochemistry	Colour + Geochemistry	FDS- PLSR	Geochemistry	Colour + geochemistry	FDS- PLSR	Geochemistry	Colour + geochemistry
1	11	90	100	56	10	0	66	100	100
2	9	94	98	58	6	2	68	100	100
3	11	89	92	52	11	8	63	100	100
4	16	69	74	66	31	26	82	100	100
5	32	82	89	54	18	11	86	100	100
6	44	81	84	51	19	16	95	100	100
7	52	77	83	36	23	17	88	100	100
8	58	83	85	35	17	15	92	100	100
Mean (%)	29	83	88	51	17	12	80	100	100
SD (%)	20	8	8	11	8	8	13	-	-
Minimum (%)	9	69	74	35	6	0	63	-	-
Maximum (%)	58	94	100	66	31	26	95	-	-

3.6 Complementary tests: representativeness of artificial mixture samples used for the FDVS-PLSR models compared to source samples

The FDVS-PLSR models provided contradictory results compared to those obtained with the 'geochemistry' and 'colour + geochemistry' models. In order to explain these results, complementary analyses were carried out with this model. This model was built from the mining and non-mining tributary samples (i.e. mixture of source samples > source poles > artificial mixture samples > FDVS-PLSR models). The objective of these analyses was to check whether the model is 'well built', in other words whether it is representative of the sources identified and whether it is capable of correctly 'classifying' the sources. To this end, we applied the FDVS-PLSR models on source samples to estimate their composition in terms of source contributions with FDVS-PLSR models. In the same way as we did above for the river sediment samples, we assessed the reliability of predictions by summing the source contributions predicted by both models (Legout et al., 2013). A mean sum of the predicted source proportions of 94 ± 17 % was calculated from the source sample data set which again is an excellent result. However, for the three mining tributary samples collected on the Koua tributary, the corresponding sums remained below 65 % with a minimum of 49 % whereas for one of the non-mining tributary sample collected on the Kouaré tributary, the sum reached 131 % (Figure 11). These results indicate that the FDVS-PLSR models provide unreliable predictions when dealing with river sediment samples with a colour signature partly due to these four samples. The colorimetric signature of the mining tributary samples collected on the Koua tributary in particular is not fully recognized by the models. The compositions of mining and non-mining tributary samples in Figures 11 and 12 also show that artificial mixture samples built from a mix between the composite mining source sample and the composite non-mining source sample did not cover entirely the range of values found in all the sources samples which may explain why some source samples showed mining and non-mining tributary composition lower than 0 and/or higher than 100 %.
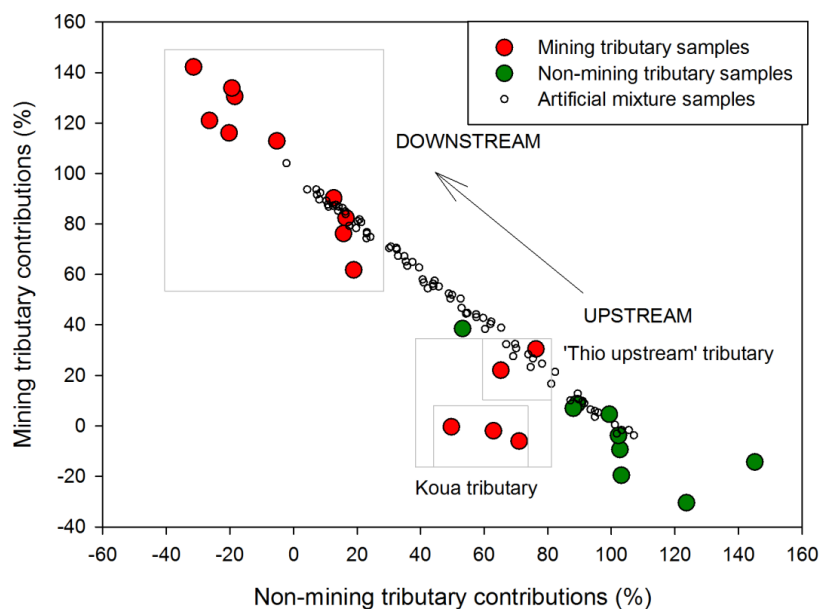
Figure 11 Relative compositions of mining and non-mining sources estimated by the FDVS-PLSR models applied to the individual source sediment samples

Moreover, we observed that two sub-groups of mining tributary samples can be distinguished, the first one corresponding to samples collected on the mining tributaries located in the uppermost part of the catchment and the second to samples collected on the mining tributaries located further downstream. The FDVS-PLSR differentiated rather well the second group since the mining tributary composition is dominant in these samples. On the contrary, the first group referred to as 'Upstream' merged with the non-mining tributary samples (Figure 11). Indeed, Figure 12 shows the mining tributaries located in the upper part of the catchment were defined as 'non-mining tributaries' by the FDVS-PLSR models.

601
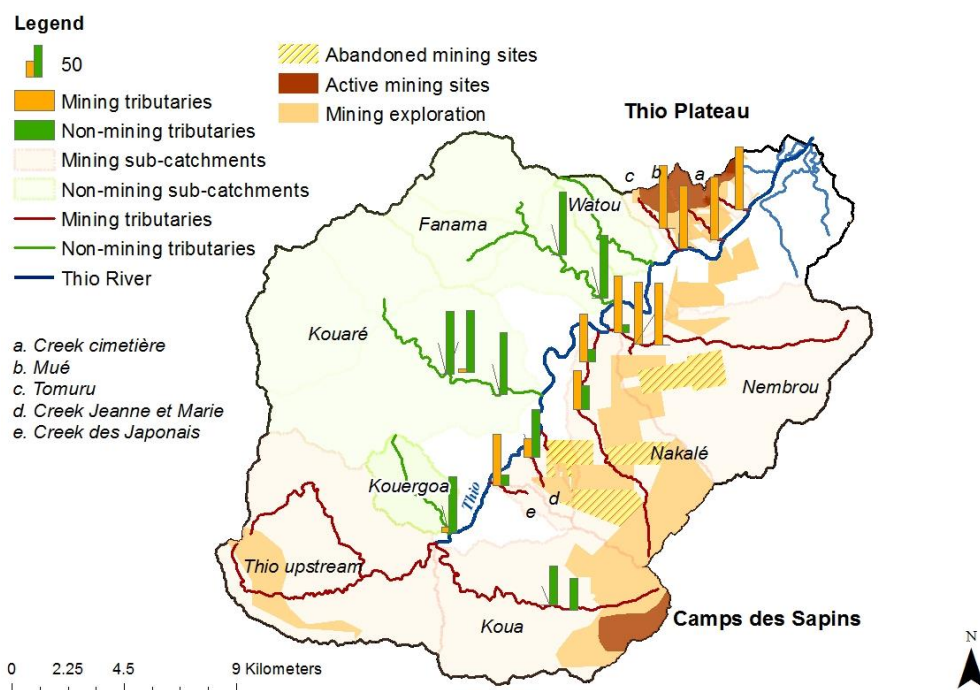
Figure 12 Relative compositions of mining and non-mining sources estimated by the FDVS-PLSR models applied to the individual sediment sources in the Thio River catchment

The low K contents found in these samples confirmed, however, that they were mainly supplied by mining sources (Figure 13). Indeed, only tributaries draining peridotite massifs (i.e. mining areas) can show such low K contents in source samples (Sellier et al., 2019). Nevertheless, a colour difference could be observed visually and through variations of the a* parameter: the a* values increased from upper parts to lower, which results in an increasingly red coloration of mining tributary samples in downstream direction. Figure 13 shows also that the a* values found in samples collected in the upper catchment part overlapped with those of non-mining tributary samples.
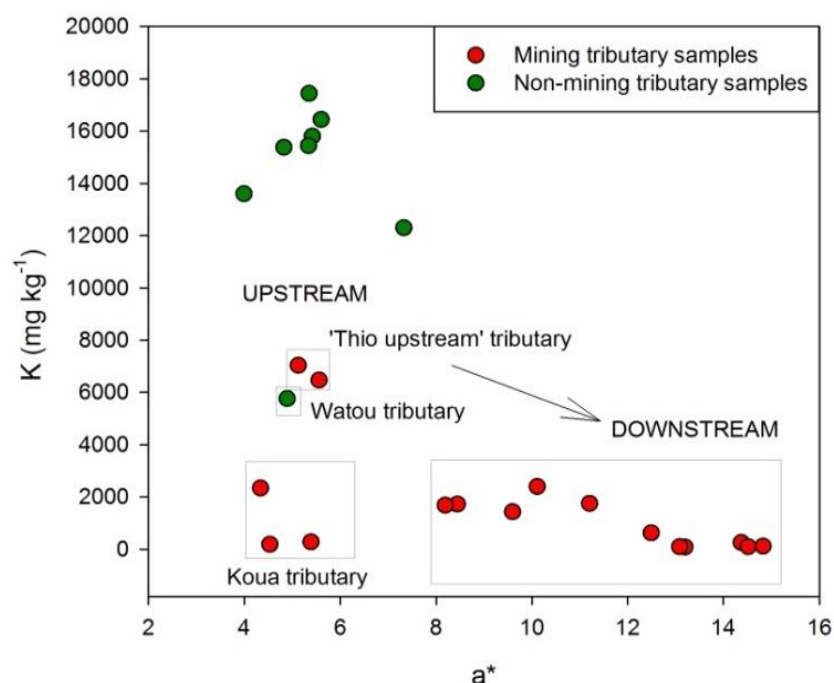
611   **Figure 13** Diagram of K contents as a function of a* parameter values within sediment sources and artificial

612   mixture samples

613   **4.Discussion**

614   **4.1 Advantages and limits of models**

615   4.1.1   'Colour' model

616   One of the objectives of this study was to test the contribution of spectrocolorimetry for

617   improving the source discrimination. Indeed, visual observations indicated that mining tributary

618   samples were red-orange whereas non-mining tributary samples were rather yellow-grey (Figure 1).

619   However, the results showed that the colour parameters, when used individually, did not provide

620   sufficient discrimination between sources (Table 2) to meet this objective. Indeed, some mining

621   tributary samples showed colour parameter values similar to those found in non-mining tributary

622   samples (e.g. v' at Table 3, or a* shown at Figure 13). This overlap of value ranges could explain in

623   particular the inability of the 'colour' model to provide satisfactory source discrimination. In the case

624   of mining sources, minerals such as hematite or goethite have a reddish-orange colour (Quantin et

625   al., 1997). Indeed, hematite is a red coloured oxidized mineral while goethite is a yellow coloured

626   oxidized mineral (Trescases, 1973). According to Figure 6, non-mining tributary samples also have

627   high contents of goethite which could interfere with the discrimination of the colour signatures of

628   the two sources. The non-mining tributaries drain areas devoid of mining activities mainly located on

629   the volcano-sedimentary formation rocks. The soil-geological profiles within the volcano-sedimentary

630   formation rocks are characterized at the surface by clay horizons and at depth by oxidized horizons

631   enriched in goethite in particular (Denis, 1988). According to Sellier et al. (2019), subsurface erosion

632   processes dominate in the Thio River catchment. In other words, landslides mainly contribute to non-

633   mining sediment inputs. As a result, the oxidized horizons of these rock formations are also likely

634   subject to erosion processes which could explain the occurrence of goethite and material with a

635   yellow-grey color in non-mining tributary samples.

636

637   Moreover, results obtained with colour parameter analyses coupled to visual observations

638   highlighted the occurrence of two groups of mining tributary samples (i.e. 'Upstream' and

639   'Downstream'). The coloration differences (i.e. orange/ 'Upstream' and 'red/Downstream') observed

640   between these two groups could be due to the the fact that on the one hand, the reddish colour

641   does not provide a highly conservative signature as it may be altered by the oxydo-reduction of iron

642   minerals during the periods of submersion of sediments under water. On the other hand, the

643   presence of different types of laterite profiles could explain these coloration differences. Indeed, the

644   laterite profile is classically described in the literature as composed of peridotites at the bottom >

645   saprolites > yellow laterites rich in goethite > red laterites rich in hematite at the top (Trescases,

646   1973). However, certain minor features may be found in the laterite profile depending on the type of

647   parent rock found at the base of the peridotite massifs (Sevin, 2014). The mineral composition found

648   in the different layers of the laterite profile may vary depending on whether serpentines or

649   peridotites are the source rocks. Moreover, laterite profile formation depends partly on the

650   morphological context, for instance on whether laterites are located in a basin, on a plateau or a

651   slope. This morphological context influences the weathering level of peridotites and the formation of

652 laterite profile: the more the laterite profile is altered, the higher the thickness of red laterites. In the

653 Thio River catchment, the laterite profile from the Thio Plateau mine located in the downstream part

654 of the catchment are 'plateau laterites' whereas those from the Camps des Sapins mine located in

655 the upstream part of the catchment are 'slope laterites' (Mardhel et al., 2018). No information is

656 provided in the literature on the types of laterite profiles that were mined in abandoned mining sites.

657 The red coloration of the 'Downstream' mining tributary samples could then be associated with more

658 altered laterite profiles with a thicker layer of red laterites characteristic of 'plateau laterites'

659 compared to the 'Upstream' mining tributary samples, which could be associated with a laterite

660 profile with a thinner layer of red laterites characteristic of 'slope laterites'. The red laterites are the

661 final stage of alteration of the peridotite massifs. It therefore appears likely that the less altered

662 'slope laterites' probably contain more yellow laterites enriched in goethite compared to the 'plateau

663 laterites'. This hypothesis could explain the similar colour signature of the mining tributary samples

664 collected on the Koua tributary draining the Camps des Sapins mine and the non-mining samples.

665   4.1.2   'Geochemistry' model

666   The 'geochemistry' model based on K provided significant discrimination between sources

667 (Table 2), regardless of the types of nickel ores that may be found in the Thio River catchment. K is a

668 lithological tracer discriminating sediments originating from the erosion of the two dominant

669 lithologies (i.e. peridotite massifs vs. volcano-sedimentary formations) in the Thio River catchment.

670 As anthropogenic erosion (i.e. due to mining activities) dominates on the peridotite massifs (Garcin

671 et al., 2017), K therefore provides an optimal discrimination between mining and non-mining

672 tributary contributions.

673   The parameter K classified the source samples rather well (i.e. 95.3 % of correct classification,

674 Table 3). Indeed, the 16 mining source samples were all correctly classified (100 %) and only one non-

675 mining source sample was not correctly classified (87.5 %); it corresponds to the Watou tributary

676 sample (Figure 13). This sample showed a K content similar to that found in mining tributary samples.

677   The Watou tributary is particular because it drains both volcano-sedimentary formations and

678   peridotite massifs that were not exploited for mining, which justifies that it was considered as a non-

679   mining tributary. The K content measured in this sample could be representative of that found in

680   sediment sources characterized by a mix between the two dominant lithologies. Again, when

681   observing Figure 13, two mining tributary samples (i.e. 'Thio upstream') showed similar K contents to

682   that found in the Watou tributary sample. The 'Thio upstream' tributary also drains both areas

683   associated with volcano-sedimentary formations and exploited peridotite massifs (i.e. mining

684   prospection), which justifies that it was considered as a mining tributary.

685   The analysis of colour parameters coupled with that of geochemical elements indicated that

686   these samples collected on the 'Thio upstream' tributary showed a less red coloration not because

687   they are associated with a different type of ore, as could be the case for the samples collected on

688   Koua tributary draining Camps des Sapins mine (Figure 13), but because they are characterized by a

689   mix of both lithologies. As a result, the 'geochemistry' model showed a certain limitation to classify

690   source samples characterized by a mix of both lithologies. The performance of the 'geochemistry'

691   model described in Table 2 remains, however, excellent. The application of this model on artificial

692   mixture samples provided very satisfactory results (Figure 5-a) with a good correlation between the

693   predicted and the actual source proportions (r^2= 0.99). Estimations of mining tributary contributions

694   may, however, be overestimated. This overestimation evaluated to a maximum at 15.5 % is greater

695   when the mining contributions estimated by the model tend towards 0 % (maximum: 15.5 %, Figure

696   3-a). The 'geochemistry' model has difficulties to discriminate sediment contributions from sub-

697   catchments with mixed lithologies. It classifies these types of samples as originating from mining

698   tributaries, such as the Watou River sample. As a result, as the K concentrations decrease in the

699   samples analyzed, the model will tend to overestimate the contributions of mining sources by default

700   compared to their actual contributions.

701

4.1.3 'Colour + geochemistry' model

The 'colour + geochemistry' (i.e. K, Ca, Ti, b*, C*) model provided the best discrimination between sources (Table 3). The inclusion of colour parameters in the 'colour + geochemistry' approach allowed for the discrimination of source samples (i.e. 100 % of correctly classified source samples) that a 'geochemistry' approach alone could not achieve. Results of the tests carried out on the artificial mixture samples also showed an excellent correlation between the predicted and the actual source proportions (i.e. $r^2 = 0.98$). A slight overestimation of the mining tributary contributions (7 %) was observed with this approach, which remains rather reasonable (Figure 3-b). In this model, K is the lithological tracer which has the higher discriminant powerful (Table 2), which may explain the similarity of results obtained with the 'colour + geochemistry' and the 'geochemistry' models. Indeed, mining tributaries contributed an average of 65 ± 27 % for 'colour + geochemistry' model and 68 ± 25 % for 'geochemistry' model (Table 4). For the 2017 flood event, mining source contributions largely dominated the sediment production with a mean contribution of 83 ± 8 % for the 'geochemistry' model and 88 ± 8 % for the 'colour + geochemistry' model.

4.1.4 FDVS-PLSR models

The FDVS-PLSR models built from artificial mixture samples showed excellent theoretical predictive performances (e.g. r^2, RMSEC, RMSEC, Figure 7). However, the application of these models on river sediment samples provided questionable results. Indeed, the artificial mixture samples did not cover entirely the ranges of values found in all sources samples, thus resulting in an overestimation (i.e. superior to 100 %) and an underestimation (i.e. inferior to 0 %) of source composition (Figure 11) in several source samples. Similarly to what was previously observed, three sub-groups of mining tributary samples can be distinguished, one of which (i.e. 'Thio Upstream') is partially merged with the non-mining tributary samples (Figure 11). When modelling the source contributions with the FDVS-PLSR models, a bias was created because the contributions of the 'Thio upstream' tributary may be mainly considered as the contributions of non-mining tributaries. As a

727   result, an overestimation of non-mining tributary contributions may be found in the entire Thio River

728   catchment and particularly in the upper part of the study area. Third, the properties measured in the

729   Koua tributary (i.e. draining Camps des Sapins Mine) samples were not comprised in the ranges of

730   values covered by the artificial mixture samples (Figure 11).

731   Given the particular colour signature of this tributary (Figure 13), its contributions are

732   therefore not taken into account at all by the FDVS-PLSR models. Indeed, the sums of the source

733   contributions by FDVS-PLSR models are lower than the expected 100 % particularly in the uppermost

734   part of the catchment (Tables 4 and 5), which may indicate that a source is not accounted for.

735   Artificial mixtures were constructed from a homogenized spectral signature of all mining source

736   samples. However, two distinct spectral signatures were observed between the upstream and

737   downstream mining source samples. Homogenizing the spectral signature of the mining samples led

738   to a loss of information in terms of spectral signature, in particular that of the mining samples

739   located upstream. As a result, a 3-source FDVS-PLSR models (i.e. non-mining, upstream and

740   downstream mining sources) would have been more appropriate than 2-source FDVS-PLSR models in

741   this context.

742   **4.2 Spatial and temporal variations of sediment source contributions**

743   Among the four models tested in this study, the 'colour + geochemistry' model is the most

744   appropriate to estimate mining and non-mining tributary contributions in the Thio River catchment.

745   According to the results of this model, mining tributaries provided the main sediment supply to the

746   river system with a mean contribution of 68 ± 25 % for the 2015 flood event and 88 ± 8 % for the

747   2017 flood event (Tables 4 and 5). The variability of mining tributary contributions between these

748   two flood events with a return period of 10 years (3500 $m^3 s^{-1}$) could be explained in particular by the

749   variability of rainfall distribution (Sellier et al., 2019). Indeed, during the 2015 flood event, the Kouaré

750   River sub-catchment received twice the rainfall than observed in the rest of the Thio River

751   catchment, which may explain a higher contribution of non-mining tributaries for this event than for

752   the 2017 flood event where rainfall was more intense on the eastern part of the catchment in the

753   vicinity of the mines currently in operation (Thio Plateau, Camps des Sapins). In addition, the

754   inhabitants of Thio reported that bushfires had occurred in the Kouaré and Fanama sub-catchments

755   in 2015, which could have led to an increase in soil erosion processes, particularly landslides, in these

756   sub-catchments. This could also explain why the sediment contributions of the Kouaré tributary are

757   higher in 2015 compared to 2017. However, it is likely that, as for low intensity floods (i.e. <200 $m^3.s^-$

758   ^{1}), sediment generated during previous floods has been remobilized (Allenbach et al., 2020). The

759   current research does not allow to quantify this proportion of remobilized sediments. Future studies

760   based on the measurement of the $^7Be/^{210}Pb_{xs}$ ratio could provide information on this question as

761   both isotopes are supplied by rainfall and ^7Be is short-lived while $^{210}Pb_{xs}$ is much longer-lived. Indeed,

762   this ratio has been used in previous research to determine whether sediment has been eroded

763   recently (i.e. with a high ratio of $^7Be/^{210}Pb_{xs}$) or whether they have been remobilized from the

764   channel (i.e.with a low ratio of $^7Be/^{210}Pb_{xs}$) (Le Gall et al., 2017;Evrard et al., 2015).

765   Although the FDVS-PLSR models were unable to properly estimate the source contributions,

766   they provided qualitative indications about the proportion of sediment contribution between

767   'Upstream' and 'Downstream' mining tributaries at the level of the estuary. Indeed, only

768   'downstream' mining tributaries were finally identified by the FDVS-PLSR models as mining sources.

769   Mining contributions gradually increased in downstream direction. The predicted proportion sums of

770   river sediment samples also tend to reach the expected 100 %, which could result in a better

771   predictability of the models. As a result, these models indicated that sediment contribution from

772   downstream reaches dominated that of upstream reaches at the level of the estuary for both events.

773   Moreover, the analysis of colour parameters coupled to that of geochemical elements

774   highlighted the occurrence of three sub-groups of mining tributary samples, (1) 'Downstream'

775   samples characterized by high a* values and low K contents, (2) 'Koua tributary' samples located in

776   the upstream characterized by low a* values and low K contents and (3) 'Thio upstream' samples

777 corresponding to a mix of both dominant lithologies (i.e. peridotite massifs and volcano-sedimentary

778 formations) characterized by low a* values and higher K contents (i.e. 4 times higher than for the

779 two previous sub-groups) (Figure 13). Owing to the low K contents found in Thio River sediment

780 samples collected in the uppermost part (i.e. ~ 2200 mg kg^{-1} in 2015 and ~ 2600 mg kg^{-1} in 2017),

781 which were similar to those measured in samples of sub-group (2) (~2400 mg kg^{-1}), it would appear

782 that the Koua tributary draining Camps des Sapins mine dominated the sediment supply in the

783 upstream for both events.

784 **Conclusions**

785   One of the objectives of this study was to evaluate the performance of sediment tracing

786 methods based on spectroscopy (i.e. colour parameters and FDVS). However, the results showed that

787 the individual fingerprinting approaches based on spectroscopy did not provide sufficient

788 discrimination between sources to be used for the modelling of sediment source contributions.

789 Nevertheless, the inclusion of colour properties in addition to geochemical parameters turned out to

790 be the optimal combination of tracers providing the highest discrimination between sediment

791 sources. This 'colour + geochemistry' model is, however largely based on the discriminatory power

792 provided by K, which explains why the results obtained between both models are so similar. Indeed,

793 the contributions of mining tributaries were estimated to 65 ± 27 % by the 'colour + geochemistry'

794 model versus 68 ± 25 % by the 'geochemistry' model for the 2015 flood event. In a similar way, the

795 contributions of mining tributaries were estimated to 88 ± 8 % by the 'colour + geochemistry' model

796 versus 83 ± 8 % by the 'geochemistry' model for the 2017 flood event. Moreover, both approaches

797 have been experimentally validated. As a result, the use of these approaches could be extended to

798 other mining catchments of New Caledonia but also possibly to other similar nickel mining areas (i.e.

799 Ni oxidized ores based on peridotite massifs) around the world. In addition, although the individual

800 fingerprinting approaches based on spectroscopy were not able to discriminate sediment sources in

801 the current research, spectroscopy measurements provided complementary information to that

802 delivered by the geochemical properties alone to discriminate between sediment sources at the

803 estuary. In the future, additional developments could be considered to improve this technique. The

804 concept of a two-source sediment tracing approach (i.e. mining vs. non-mining tributary

805 contributions) may be too simplistic in a mining context. The initial hypothesis that red-orange

806 eroded sediment comes from mining tributaries whereas yellow-grey material originates from non-

807 mining tributaries could not be fully confirmed in New Caledonia. Indeed, soils found in both mining

808 and non-mining areas are all highly weathered and share similarities in terms of oxidized mineral

809 composition (e.g. goethite), which likely generates confusion for discriminating their respective

810 colorimetric signatures. Moreover, soils found across all mining areas across a single catchment are

811 not necessarily identical, as different depths of their respective weathering profiles may crop out and

812 result in variable colorimetric signatures. A preliminary identification of these soils characteristic of

813 different weathering stages could be considered to improve the results of sediment tracing

814 approaches based on spectroscopic measurements, both in New Caledonia and in other similar nickel

815 mining catchments around the world.

Data availability

817 The database has been registered on the PANGEAE website and is currently undergoing the

818 editorial process: https://issues.pangaea.de/browse/PDI-25229.

Author contribution

820 Oldrich Navratil, Michel Allenbach and Olivier Evrard designed research. Virginie Sellier,

821 Oldrich Navratil, Olivier Evrard and Irène Lefèvre carried out fieldwork sampling. Virginie Sellier

822 conducted the analyses. All co-authors contributed to data analysis and interpretation. John Patrick

823 Laceby contributed to modelling. All co-authors contributed to the writing and approved the final

824 version of the manuscript.

825 **Competing interests**

826 The authors declare that they have no conflict interest.

827 **Acknowledgements**

828 This work was funded by the National Technical Research Center (CNRT) "Nickel and Its

829 Environment", Noumea, New Caledonia » (n°10PS2013-CNRT.UNC/IMMILA). The PhD project of

830 Virginie Sellier is also financed by the French Atomic Energy Commission (CEA, Commissariat à

831 l'Energie Atomique et aux Energies Alternatives). The authors are grateful to Jean-Guy M'Boueri,

832 Pierre Chanel, Jean-Jean, Lorenza M'Boueri, Nicolle Mathys for their invaluable support to identify

833 and have access to the field sampling sites. The authors would also like to thank Magdalena Uber for

834 her contribution to the spectrocolorimetric analyses.

835

References

836 **References**

837 Abel, A., Michael, A., Zartl, A., and Werner, F.: Impact of erosion-transported overburden dump
838   materials on water quality in Lake Cospuden evolved from a former open cast lignite mine
839   south of Leipzig, Germany, Environmental Geology, 39, 683-688, 2000.

840 Allenbach, M., Bertrand, M., Despinoy, Y., Evrard, O., Garcin, M., Liébault, F., Navratil, O., Recking, A.,
841   Richard, D., Rouet, I., Sabinot, C., Sellier, V., Tessier, B., Thinon, I., Touraivane, and Worliczek,
842   E.: Rapport scientifique. Programme « IMMILA, Impact de la mine au lagon ». CNRT « Nickel
843   & son environnement. 250 pages. , 2020.

844 Batista, P. V. G., Laceby, J. P., Silva, M. L. N., Tassinari, D., Bispo, D. F. A., Curi, N., Davies, J., and
845   Quinton, J. N.: Using pedological knowledge to improve sediment source apportionment in
846   tropical environments, J Soils Sediments, 10.1007/s11368-018-2199-5, 2018.

847 Baudrimont, M., Dominique, Y., Feurtet-Mazel, A., Gonzalez, P., Gourvès, P.-Y., Gunkel-Grillon, P.,
848   Laporte-Magoni, C., Lefrançois, E., Letourneur, Y., Marquié, J., Maury-Brachet, R., Monna, F.,
849   Pasquet, C., Rivière, E., and Roth, E.: - Rapport scientifique final. Programme « Dispersion des
850   métaux de la mine au lagon. ». CNRT « Nickel & son environnement ». 192 pages, 2019.

851 Bird, E. C. F., Dubois, J. P., and Iltis, J. A.: The impacts of opencast mining on the rivers and coasts of
852   New Caledonia. Tokyo, Japan, United Nations University, 1984.

853 Blake, W. H., Wallbrink, P. J., Wilkinson, S. N., Humphreys, G. S., Doerr, S. H., Shakesby, R. A., and
854   Tomkins, K. M.: Deriving hillslope sediment budgets in wildfire-affected forests using fallout
855   radionuclide tracers, Geomorphology, 104, 105-116, 10.1016/j.geomorph.2008.08.004, 2009.

856 Brosinsky, A., Foerster, S., Segl, K., and Kaufmann, H.: Spectral fingerprinting: sediment source
857   discrimination and contribution modelling of artificial mixtures based on VNIR-SWIR spectral
858   properties, Journal of soils and sediments, 14, 1949-1964, 2014.

859 Brown, A.: The potential use of pollen in the identification of suspended sediment sources, Earth
860   Surface Processes and Landforms, 10, 27-32, 1985.

861 Clarke, P., and David, C.: New Provincial Environmental Legislation in New Caledonia: Continuity and
862   Reform in Environmental Governance in a French Pacific Territory, Asia Pac. J. Envtl. L., 13,
863   135, 2010.

864 Collins, A., and Walling, D.: Selecting fingerprint properties for discriminating potential suspended
865   sediment sources in river basins, Journal of hydrology, 261, 218-244, 2002.

866 Collins, A. L., Walling, D. E., and Leeks, G. J. L.: Composite fingerprinting of the spatial source of fluvial
867   suspended sediment : a case study of the Exe and Severn river basins, United Kingdom,
868   Géomorphologie, 2, 41-53, 10.3406/morfo.1996.877, 1996.

869 Coulthard, T. J., and Macklin, M. G.: Modeling long-term contamination in river systems from
870   historical metal mining, Geology, 31, 451-454, 2003.

871 Danloux, J., and Laganier, R.: Classification et quantification des phénomènes d'érosion, de transport
872   et de sédimentation sur les bassins touchés par l'exploitation minière en Nouvelle Calédonie,
873   1991.

874 Daszykowski, M., Walczak, B., and Massart, D.: Representative subset selection, Analytica chimica
875   acta, 468, 91-103, 2002.

876 Davis, C. M., and Fox, J. F.: Sediment fingerprinting: review of the method and future improvements
877   for allocating nonpoint source pollution, J Environ Eng, 135, 490-504, 2009.

878 Debret, M., Sebag, D., Desmet, M., Balsam, W., Copard, Y., Mourier, B., Susperrigui, A.-S., Arnaud, F.,
879   Bentaleb, I., and Chapron, E.: Spectrocolorimetric interpretation of sedimentary dynamics:
880   the new "Q7/4 diagram", Earth-Science Reviews, 109, 1-19, 2011.

881 Denis, B.: Etude de sols fersiallitiques désaturés du plateau de Tango (Nouvelle-Calédonie), Cahiers
882   ORSTOM. Série Pédologie, 24, 61-76, 1988.

883 Dumas, P.: Méthodologie de cartographie de la sensibilité des sols à l'érosion appliquée à la région
884   de Dumbéa à Païta-Bouloupari (Nouvelle-Calédonie), Les Cahiers d'Outre-Mer. Revue de
885   géographie de Bordeaux, 63, 567-584, 2010.

886 Dumas, P., Printemps, J., Mangeas, M., and Luneau, G.: Developing erosion models for integrated
887   coastal zone management: A case study of The New Caledonia west coast, Marine Pollution
888   Bulletin, 61, 519-529, 2010.

889 Evrard, O., Laceby, J. P., Huon, S., Lefèvre, I., Sengtaheuanghoung, O., and Ribolzi, O.: Combining
890   multiple fallout radionuclides (137Cs, 7Be, 210Pbxs) to investigate temporal sediment source
891   dynamics in tropical, ephemeral riverine systems, J Soils Sediments, 16, 1130-1144,
892   10.1007/s11368-015-1316-y, 2015.

893 Evrard, O., Durand, R., Foucher, A., Tiecher, T., Sellier, V., Onda, Y., Lefèvre, I., Cerdan, O., and
894   Laceby, J. P.: Using spectrocolourimetry to trace sediment source dynamics in coastal
895   catchments draining the main Fukushima radioactive pollution plume (2011–2017), Journal
896   of Soils and Sediments, 1-12, 2019.

897 Evrard, O., Chaboche, P.-A., Ramon, R., Foucher, A., and Laceby, J. P.: A global review of sediment
898   source fingerprinting research incorporating fallout radiocesium (137Cs), Geomorphology,
899   107103, 2020.

900 Garcin, M.: Exploitation des granulats en lit vif des cours d'eau de la Grande-Terre, Nouvelle-
901   Calédonie. BRGM/RP-58531-FR. 114 p., 90 fig., 3 tabl., Bureau des Recherches Géologiques et
902   Minières 2010.

903 Garcin, M., Gastaldi, Y., and Lesimple, S.: Quantification et évolution temporelle des apports miniers
904   dans les rivières calédoniennes. BRGM/RP-66840-FR, 44 p., 23 fig., 5, Bureau des Recherches
905   Géologiques et Minières

906 2017.

907 Gruszowski, K., Foster, I. D., Lees, J., and Charlesworth, S.: Sediment sources and transport pathways
908   in a rural catchment, Herefordshire, UK, Hydrological Processes, 17, 2665-2681, 2003.

909 Hedouin, L., Pringault, O., Metian, M., Bustamante, P., and Warnau, M.: Nickel bioaccumulation in
910   bivalves from the New Caledonia lagoon: Seawater and food exposure, Chemosphere, 66,
911   1449-1457, 2007.

912 Highley, D., Chapman, G. R., and Bonel, K.: The economic importance of minerals to the UK, British
913   Geological Survey, 2004.

914 Iltis, J.: La mine, élement de la controverse écologique dans le Pacifique Sud, L'Espace géographique,
915   193-205, 1992.

916 James, L. A.: Legacy sediment: definitions and processes of episodically produced anthropogenic
917   sediment, Anthropocene, 2, 16-26, 2013.

918 Juillot, F.: – Rapport scientifique final. Programme « Dynamique des métaux de la mine au lagon ».
919   CNRT « Nickel & son environnement ». 202 pages., 2019.

920 Klages, M., and Hsieh, Y.: Suspended Solids Carried by the Gallatin River of Southwestern Montana:
921   II. Using Mineralogy for Inferring Sources 1, Journal of Environmental Quality, 4, 68-73, 1975.

922 Kumar, A., and Maiti, S. K.: Assessment of potentially toxic heavy metal contamination in agricultural
923   fields, sediment, and water from an abandoned chromite-asbestos mine waste of Roro hill,
924   Chaibasa, India, Environmental earth sciences, 74, 2617-2633, 2015.

925 Laceby, J. P., and Olley, J.: An examination of geochemical modelling approaches to tracing sediment
926   sources incorporating distribution mixing and elemental correlations, Hydrol. Process., 29,
927   1669-1685, 10.1002/hyp.10287, 2015.

928 Laceby, J. P., Evrard, O., Smith, H. G., Blake, W. H., Olley, J. M., Minella, J. P. G., and Owens, P. N.: The
929   challenges and opportunities of addressing particle size effects in sediment source
930   fingerprinting: A review, Earth-Sci. Rev., 169, 85-103, 10.1016/j.earscirev.2017.04.009, 2017.

931 Le Gall, M., Evrard, O., Foucher, A., Laceby, J. P., Salvador-Blanes, S., Manière, L., Lefèvre, I., Cerdan,
932   O., and Ayrault, S.: Investigating the temporal dynamics of suspended sediment during flood
933   events with 7 Be and 210 Pb xs measurements in a drained lowland catchment, Scientific
934   reports, 7, 42099, 2017.

935 Legout, C., Poulenard, J., Nemery, J., Navratil, O., Grangeon, T., Evrard, O., and Esteves, M.:
936   Quantifying suspended sediment sources during runoff events in headwater catchments
937   using spectrocolorimetry, J Soils Sediments, 13, 1478-1492, 10.1007/s11368-013-0728-9,
938   2013.

939 Mardhel, V., Iseppi, M., Regninger, P. A., and Sevin, B.: Connaissance de l'ophiolite, géophysique
940   aéroportée et étude de la structure. Rapport scientifique final. Programme «OPHIOSTRUCT».
941   CNRT «Nickel & son environnement», 2018.

942 Martínez-Carreras, N., Udelhoven, T., Krein, A., Gallart, F., Iffly, J. F., Ziebel, J., Hoffmann, L., Pfister,
943   L., and Walling, D. E.: The use of sediment colour measured by diffuse reflectance
944   spectrometry to determine sediment sources: application to the Attert River catchment
945   (Luxembourg), J Hydrol, 382, 49-63, 2010.

946 Motha, J., Wallbrink, P., Hairsine, P., and Grayson, R.: Unsealed roads as suspended sediment sources
947   in an agricultural catchment in south-eastern Australia, Journal of Hydrology, 286, 1-18,
948   2004.

949 Navratil, O., Evrard, O., Esteves, M., Legout, C., Ayrault, S., Némery, J., Mate-Marin, A., Ahmadi, M.,
950   Lefèvre, I., and Poirel, A.: Temporal variability of suspended sediment sources in an alpine

951   catchment combining river/rainfall monitoring and sediment fingerprinting, Earth Surface
952   Processes and Landforms, 37, 828-846, 2012.

953 Owens, P. N., and Walling, D. E.: The phosphorus content of fluvial sediment in rural and
954   industrialized river basins, Water Res., 36, 685-701, 2002.

955 Pascal, N.: Ecosystèmes coralliens de Nouvelle-Calédonie. Valeur économique des services
956   écosystémiques. Partie I: Valeur financière. IFRECOR., 2010.

957 Poulenard, J., Perrette, Y., Fanget, B., Quetin, P., Trevisan, D., and Dorioz, J.-M.: Infrared
958   spectroscopy tracing of sediment sources in a small rural watershed (French Alps), Science of
959   the Total Environment, 407, 2808-2819, 2009.

960 Poulenard, J., Legout, C., Nemery, J., Bramorski, J., Navratil, O., Douchin, A., Fanget, B., Perrette, Y.,
961   Evrard, O., and Esteves, M.: Tracing sediment sources during floods using Diffuse Reflectance
962   Infrared Fourier Transform Spectrometry (DRIFTS): A case study in a highly erosive
963   mountainous catchment (Southern French Alps), Journal of Hydrology, 414, 452-462, 2012.

964 Priadi, C., Ayrauk, S., Pacini, S., and Bonte, P.: Urbanization impact on metals mobility in riverine
965   suspended sediment: role of metal oxides, International Journal of Environmental Science &
966   Technology, 8, 1-18, 2011.

967 Prior, T., Daly, J., Mason, L., and Giurco, D.: Resourcing the future: Using foresight in resource
968   governance, Geoforum, 44, 316-328, 2013.

969 Quantin, P., Bourdon, E., and Becquer, T.: Minéralogie et contraintes édaphiques des sols"
970   ferritiques" dérivés de roches ultrabasiques en Nouvelle-Calédonie: relations entre
971   constituants minéraux et disponiblté en certains éléments (Al, Fe, Si, Mg, Mn, Ni, Co, Cr, Cu,
972   Zn, Mo) facilement solubles, 1997.

973 Rossel, R. V., Walvoort, D., McBratney, A., Janik, L. J., and Skjemstad, J.: Visible, near infrared, mid
974   infrared or combined diffuse reflectance spectroscopy for simultaneous assessment of
975   various soil properties, Geoderma, 131, 59-75, 2006.

976 Sellier, V., Navratil, O., Laceby, J. P., Allenbach, M., Lefèvre, I., and Evrard, O.: Investigating the use of
977   fallout and geogenic radionuclides as potential tracing properties to quantify the sources of
978   suspended sediment in a mining catchment in New Caledonia, South Pacific, Journal of Soils
979   and Sediments, 1-17, 2019.

980 Sevin, B.: Cartographie du régolithe sur formation ultrabasique de Nouvelle-Calédonie: Localisation
981   dans l'espace et le temps des gisements nickélifères, Nouvelle Calédonie, 2014.

982 Shellberg, J., Brooks, A., and Spencer, J.: Land-use change from indigenous management to cattle
983   grazing initiates the gullying of alluvial soils in northern Australia, 19th World Congress of Soil
984   Science: Soil Solutions for a Changing World, 2010, 1-6,

985 Sherriff, S. C., Franks, S. W., Rowan, J. S., Fenton, O., and Ó'hUallacháin, D.: Uncertainty-based
986   assessment of tracer selection, tracer non-conservativeness and multiple solutions in
987   sediment fingerprinting using synthetic and field data, J Soils Sediments, 15, 2101-2116,
988   10.1007/s11368-015-1123-5, 2015.

989 Smith, H. G., Sheridan, G. J., Lane, P. N. J., Noske, P. J., and Heijnis, H.: Changes to sediment sources
990   following wildfire in a forested upland catchment, southeastern Australia, Hydrol. Process.,
991   25, 2878-2889, 10.1002/hyp.8050, 2011.

992 Surell, A.: Étude sur les torrents des Hautes-Alpes, Carilian-Goeury, 1841.

993 Tiecher, T., Caner, L., Minella, J. P., and dos Santos, D. R.: Combining visible-based-color parameters
994   and geochemical tracers to improve sediment source discrimination and apportionment, Sci
995   Total Environ, 527-528, 135-149, 10.1016/j.scitotenv.2015.04.103, 2015.

996 Trescases, J. J.: Weathering and geochemical behaviour of the elements of ultramafic rocks in New
997   Caledonia, BMRJ. Aust. Geol and Geophys., 141, 149-161, 1973.

998 Uber, M., Legout, C., Nord, G., Crouzet, C., Demory, F., and Poulenard, J.: Comparing alternative
999   tracing measurements and mixing models to fingerprint suspended sediment sources in a
1000   mesoscale Mediterranean catchment, Journal of Soils and Sediments, 1-19, 2019.

1001 Valette-Silver, N. J.: The use of sediment cores to reconstruct historical trends in contamination of
1002   estuarine and coastal sediments, Estuaries, 16, 577-588, 1993.

1003 Varol, M.: Assessment of heavy metal contamination in sediments of the Tigris River (Turkey) using
1004   pollution indices and multivariate statistical techniques, Journal of Hazardous Materials, 195,
1005   355-364, 2011.

1006 Wallbrink, P., Murray, A., Olley, J., and Olive, L.: Determining sources and transit times of suspended
1007   sediment in the Murrumbidgee River, New South Wales, Australia, using fallout 137Cs and
1008   210Pb, Water Resour Res, 34, 879-887, 1998.

1009 Wallbrink, P. J.: Quantifying the erosion processes and land-uses which dominate fine sediment
1010   supply to Moreton Bay, Southeast Queensland, Australia, Journal of environmental
1011   radioactivity, 76, 67-80, 2004.

1012 Walling, D., Peart, M., Oldfield, F., and Thompson, R.: Suspended sediment sources identified by
1013   magnetic measurements, Nature, 281, 110, 1979.

1014 Yellishetty, M., Mudd, G. M., and Shukla, R.: Prediction of soil erosion from waste dumps of opencast
1015   mines and evaluation of their impacts on the environment, International Journal of Mining,
1016   Reclamation and Environment, 27, 88-102, 2013.

1017